



**HAL**  
open science

## Digestion of Chromatin in Apoptotic Cell Microparticles Prevents Autoimmunity

Vanja Sisirak, Benjamin Sally, Vivette d'Agati, Wilnelly Martinez-Ortiz, Z Birsin Özçakar, Joseph David, Ali Rashidfarrokhi, Ada Yeste, Casandra Panea, Asiya Seema Chida, et al.

### ► To cite this version:

Vanja Sisirak, Benjamin Sally, Vivette d'Agati, Wilnelly Martinez-Ortiz, Z Birsin Özçakar, et al.. Digestion of Chromatin in Apoptotic Cell Microparticles Prevents Autoimmunity. *Cell*, 2016, 166 (1), pp.88 - 101. 10.1016/j.cell.2016.05.034 . hal-03045372

**HAL Id: hal-03045372**

**<https://hal.science/hal-03045372>**

Submitted on 27 Jan 2021

**HAL** is a multi-disciplinary open access archive for the deposit and dissemination of scientific research documents, whether they are published or not. The documents may come from teaching and research institutions in France or abroad, or from public or private research centers.

L'archive ouverte pluridisciplinaire **HAL**, est destinée au dépôt et à la diffusion de documents scientifiques de niveau recherche, publiés ou non, émanant des établissements d'enseignement et de recherche français ou étrangers, des laboratoires publics ou privés.

## **Digestion of Chromatin in Apoptotic Cell Microparticles Prevents Autoimmunity**

Vanja Sisirak<sup>1\*</sup>, Benjamin Sally<sup>1,2\*</sup>, Vivette D'Agati<sup>3</sup>, Wilnelly Martinez-Ortiz<sup>4</sup>, Z. Birsin Özçakar<sup>5</sup>, Joseph David<sup>1</sup>, Ali Rashidfarrokhi<sup>1</sup>, Ada Yeste<sup>6</sup>, Casandra Panea<sup>2</sup>, Asiya Seema Chida<sup>8</sup>, Milena Bogunovic<sup>7</sup>, Ivaylo I. Ivanov<sup>2</sup>, Francisco J. Quintana<sup>6</sup>, Inaki Sanz<sup>8</sup>, Keith B. Elkon<sup>9</sup>, Mustafa Tekin<sup>10</sup>, Fatoş Yalçınkaya<sup>5</sup>, Timothy J. Cardozo<sup>4</sup>, Robert M. Clancy<sup>11</sup>, Jill P. Buyon<sup>11</sup> and Boris Reizis<sup>1,2,11</sup>

<sup>1</sup>Dept. of Pathology, New York University School of Medicine, New York, NY; <sup>2</sup>Dept. of Microbiology and Immunology, Columbia University Medical Center, New York, NY; <sup>3</sup>Dept. of Pathology, Columbia University Medical Center, New York, NY; <sup>4</sup>Dept. of Biochemistry and Molecular Pharmacology, New York University School of Medicine, New York, NY; <sup>5</sup>Dept. of Pediatrics, Division of Pediatric Nephrology, Ankara University School of Medicine, Ankara, Turkey; <sup>6</sup>Ann Romney Center for Neurologic Diseases, Brigham and Women's Hospital, Harvard Medical School, Boston, MA; <sup>7</sup>Dept. of Microbiology and Immunology, Milton S. Hershey Medical Center, Pennsylvania State University, Hershey, PA; <sup>8</sup>Dept. of Medicine, Division of Rheumatology, Emory University, Atlanta, GA; <sup>9</sup>Dept. of Medicine, University of Washington, Seattle, WA; <sup>10</sup>Dept. of Human Genetics, Miller School of Medicine, University of Miami, Miami, FL; <sup>11</sup>Department of Medicine, New York University School of Medicine, New York, NY, USA.

\* these authors contributed equally

Correspondence: B.R. (Boris.Reizis@nyumc.org)

### **Summary**

Antibodies to DNA and chromatin drive autoimmunity in systemic lupus erythematosus (SLE). Null mutations and hypomorphic variants of the secreted DNASE1-like deoxyribonuclease DNASE1L3 are linked to familial and sporadic SLE, respectively. We report that *Dnase1/3*-deficient mice rapidly develop autoantibodies to DNA and chromatin, followed by SLE-like inflammatory disease. Anti-DNA autoreactivity was independent of STING-mediated intracellular DNA sensing and inversely correlated with the levels of circulating DNASE1L3. Circulating DNASE1L3 was produced primarily by dendritic cells and macrophages. Due to its ability to digest nucleosomal and lipid-associated DNA, DNASE1L3 was capable of digesting chromatin in microparticles released from apoptotic cells. Circulating microparticles in *Dnase1/3*-deficient mice and human patients were overloaded with genomic DNA. DNASE1L3-sensitive chromatin on the surface of microparticles was targeted by SLE autoantibodies in murine and human SLE. Thus, processing of chromatin in apoptotic microparticles by secreted DNASE1L3 is a fundamental mechanism of tolerance to self-DNA that prevents systemic autoimmunity.

### **Highlights**

- \* Rapid anti-DNA antibody response followed by SLE in *Dnase1/3*-deficient mice
- \* Autoreactivity is repressed by circulating DNASE1L3 and is independent of STING
- \* DNASE1L3 digests genomic DNA in microparticles released from apoptotic cells
- \* DNASE1L3 prevents autoantibody binding to chromatin on microparticle surface

## Introduction

The hallmark of systemic lupus erythematosus (SLE) is the production of antibodies to nuclear antigens such as ribonucleoproteins and DNA. Autoantibody production by self-reactive B cells triggers and is further amplified by the activation of innate immune system, including myeloid cell activation and secretion of type I interferon (interferon  $\alpha/\beta$ , IFN) (Choi et al., 2012; Elkon and Wiedeman, 2012; Fairhurst et al., 2006). Ultimately, autoantibodies forming immune complexes with nucleic acids are deposited in tissues, where they cause chronic inflammatory conditions such as vasculitis and glomerulonephritis. High-affinity IgG antibodies to double-stranded DNA (dsDNA) are thought to be particularly pathogenic and associated with the severity of glomerulonephritis in SLE (Pisetsky, 2016). Furthermore, antibodies to chromatin including nucleosomes are common in SLE and may serve as especially sensitive biomarkers of the disease (Bizzaro et al., 2012; Rekvig et al., 2014). Thus, the loss of B cell tolerance to genomic DNA within chromatin represents a major mechanism of SLE pathogenesis.

B cells with DNA-reactive antigen receptors are present in the normal lymphocyte repertoire, particularly among “innate-like” B cell populations such as marginal zone B (MZB) cells and B-1 cells (Sang et al., 2013; Wardemann and Nussenzweig, 2007). Therefore, one major question concerns the physical form(s) of DNA that can be recognized by autoreactive B cells in SLE and the mechanisms that prevent such recognition in normal conditions. DNA from apoptotic cells is degraded by the intracellular enzyme DNASE2, whose deletion in mice causes fulminant IFN-driven autoinflammation (Nagata and Kawane, 2011). Similarly, DNA of reverse-transcribed retroelements is degraded by an intracellular exonuclease TREX1, and the loss of

TREX1 causes IFN-driven inflammatory disease in human patients (Aicardi-Goutieres syndrome) and in mice (Crow, 2015; Volkman and Stetson, 2014). Importantly, these inflammatory conditions are driven by innate DNA sensing that requires the cytoplasmic protein STING (Ahn et al., 2012; Gall et al., 2012) rather than by DNA-specific B cells. Another potentially immunogenic form of genomic DNA is neutrophil extracellular traps (NETs) released by activated granulocytes. These NETs may engage endosomal Toll-like receptor TLR9 (Garcia-Romo et al., 2011; Lande et al., 2011) or STING (Lood et al., 2016) to induce IFN production. However, it is unclear whether NETs can serve as antigens for autoreactive B cells, and their role in experimental SLE needs further investigation (Campbell et al., 2012). Finally, genomic DNA of apoptotic cells is incorporated into membrane-coated microparticles (Pisetsky et al., 2010), which are normally present in the plasma of healthy subjects and SLE patients (Dieker et al., 2016; Nielsen et al., 2011; Nielsen et al., 2012). These microparticles were shown to expose chromatin on their surface (Ullal et al., 2014; Ullal et al., 2011), and therefore might represent potential antigens for DNA-reactive B cells. However, the relationship of microparticle DNA to total DNA in human plasma (Snyder et al., 2016; Sun et al., 2015), its regulation and potential role in SLE remain obscure.

A recent study (Al-Mayouf et al., 2011) identified several Saudi Arabian families with a high incidence of aggressive SLE with anti-dsDNA reactivity in children. The phenotype segregated with homozygosity for the same frameshift mutation in the *DNASE1L3* gene. A subsequent study (Ozcarar et al., 2013) identified two independent *DNASE1L3* mutations in Turkish families with autosomal-recessive hypocomplementemic urticarial vasculitis syndrome (HUVS). HUVS is often associated with SLE, and indeed 3 out of 4 surviving *DNASE1L3*-deficient children developed

severe SLE with anti-dsDNA. Furthermore, previously described strong associations of the *PXK* gene with SLE and other systemic autoimmune diseases have been recently re-assigned to the adjacent *DNASE1L3* gene (Mayes et al., 2014; Zochling et al., 2014). The disease-associated *DNASE1L3* polymorphism (*rs35677470*) creates an amino acid substitution (R206C) that appears to reduce DNase activity (Ueki et al., 2009). Thus, the loss of *DNASE1L3* causes familial autosomal-recessive SLE, and in parallel, the hypomorphic *DNASE1L3* allele is associated with common sporadic SLE. These data establish *DNASE1L3* as a critical genetic determinant of SLE susceptibility and an essential factor protecting humans from the disease.

*DNASE1L3* belongs to the family of DNases homologous to *DNASE1*, a secreted DNase dedicated to processing ingested DNA in the gastrointestinal tract (Baron et al., 1998; Shiokawa and Tanuma, 2001). *DNASE1* and *DNASE1L3* together are responsible for most of the DNase activity in serum (Napirei et al., 2009). However, unlike *DNASE1* or its other homologs, *DNASE1L3* contains a short C-terminal peptide that is positively charged and resembles cell-penetrating peptides. Indeed, this peptide allows *DNASE1L3* to digest DNA encapsulated into artificial membranes such as liposomes (Wilber et al., 2002). In addition, *DNASE1L3* is more efficient than *DNASE1* in the internucleosomal cleavage of genomic DNA in isolated cell nuclei (Napirei et al., 2005), suggesting that it might facilitate the digestion of chromatin within apoptotic or necrotic cells (Mizuta et al., 2013). However, neither the natural form of DNA targeted by *DNASE1L3* nor the mechanism whereby *DNASE1L3* protects from SLE have been elucidated.

Here we show that the loss of *DNASE1L3* in mice caused a rapid and fully penetrant antibody response to dsDNA and chromatin. The resulting disease resembled

classical SLE rather than IFN-driven inflammatory disease, and arose independently of DNA sensing through STING. We also found that DNASE1L3 is uniquely capable of digesting chromatin in apoptotic cell-derived microparticles, and its absence caused the accumulation of and antibody response to microparticle-associated DNA. These results suggest that chromatin in apoptotic microparticles represents an important antigenic form of DNA in SLE, and identify DNASE1L3 as the factor that restricts their immunogenicity in the steady state.

## Results

### ***Dnase1l3-deficient mice rapidly develop anti-DNA autoantibodies***

We analyzed mice in which essential coding exons of the *Dnase1l3* gene have been replaced with a *LacZ* reporter cassette (Fig. S1A). The *Dnase1l3*<sup>LacZ</sup> allele was crossed onto two common inbred backgrounds, C57BL/6 (B6) and 129SvEv (129). Homozygous *Dnase1l3*<sup>LacZ/LacZ</sup> knockout (KO) mice were born at Mendelian ratios and were grossly normal and fertile. All examined KO mice but none of the WT mice on both B6 and 129 backgrounds developed anti-nuclear antibodies (ANA) with perinuclear staining (Fig. 1A), which is characteristic of acute human SLE with anti-dsDNA. The titers of anti-dsDNA IgG in the sera of KO mice were elevated starting at 5 weeks of age, with subsequent increase in all KO mice on both backgrounds (Fig. 1B). Both male and female KO mice developed ANA and anti-dsDNA with the same kinetics, although females manifested higher anti-dsDNA titers (data not shown). No significant increase in anti-dsDNA IgM was detected in KO mice (data not shown). Anti-dsDNA primarily comprised IgG2a and IgG2b isotypes that are known to be pathogenic in other SLE models (Ehlers et al., 2006) (Fig. 1C). ELISPOT analysis revealed an abundance of

anti-dsDNA IgG antibody-secreting cells (ASC) in KO mice on both backgrounds (Fig. 1D). Moreover, anti-dsDNA ASC were significantly expanded in KO spleens as early as at 4-6 weeks of age (Fig. 1E). In contrast, neither total immunoglobulins nor anti-RNA IgG were elevated even in old mice (Fig. S1B,C). The analysis of KO sera by autoantigen microarray and ELISA revealed increased reactivity to several protein and ribonucleoprotein autoantigens at 40 weeks but not earlier (Fig. S1D-F).

Given the emerging importance of anti-chromatin antibodies in SLE, we tested IgG reactivity to native polynucleosomes purified from cultured cells. KO mice rapidly developed high titers of anti-chromatin IgG on both 129 and B6 backgrounds (Fig. 1F and data not shown). No reactivity to purified histones was observed, suggesting that anti-chromatin IgG react to dsDNA-containing nucleosomes (not shown). The analysis of a synchronized cohort of KO mice showed that anti-chromatin IgG developed even more rapidly than anti-dsDNA IgG at 5 weeks (Fig. 1G,H). Thus, *Dnase1/3*-deficient mice manifest rapid and specific responses to dsDNA and chromatin, whereas the response to other antigens is absent or delayed. These data suggest that the endogenous genomic DNA represents the primary autoantigen in this model.

### ***Dnase1/3*-deficient mice develop features of SLE**

We analyzed *Dnase1/3*-deficient mice for signs of immune activation and tissue inflammation. Peripheral blood of KO mice on both backgrounds harbored a progressively increasing fraction of CD11c<sup>+</sup> MHC class II<sup>-</sup> myeloid cells (Fig. 2A,B). The phenotype of these cells (CD11c<sup>lo</sup> MHC class II<sup>-</sup> CD11b<sup>+</sup> Ly-6C<sup>-</sup>) matches Gr-1<sup>-</sup> monocytes that express FcγRIV and are expanded in other SLE models (Santiago-Raber et al., 2009). By 50 weeks of age, KO mice manifested splenomegaly (Fig. 2C,D)

with reduced MZB population and increased fractions of splenic monocytes and activated T cells (Fig. S2A-C). The enlarged spleens showed spontaneous germinal center (GC) formation and an increased fraction of GC B cells (significant on the 129 background, Fig 2E,F). All 50-week-old KO mice on both backgrounds showed IgG deposition in the kidney glomeruli (Fig. 2G). Finally, KO mice on the 129 background developed glomerulonephritis including enlargement of glomeruli, mesangial and endocapillary proliferation, glomerular deposits and interstitial inflammation of the kidney cortex (Fig. 2H,I). KO mice on the B6 background showed glomerular enlargement but no overt glomerulonephritis. Thus, anti-DNA response in *Dnase1/3*-deficient mice is followed by immune activation, IgG deposition and a background-dependent glomerulonephritis.

In contrast to the early onset of anti-DNA response, the observed immune activation was largely absent from KO mice up to 27 weeks of age (Fig. 2D-E and S2A-C). The development of experimental SLE can be accelerated by a surge in IFN production, e.g. after the adenoviral delivery of IFN (Mathian et al., 2005). We therefore injected young KO or control mice with the adenoviral vector encoding IFN- $\alpha$ 5, resulting in elevated serum IFN and elevated expression of IFN-inducible protein Sca-1 for at least 5 weeks post-injection (Fig. S2D,E). IFN-treated KO mice showed rapid accrual of anti-dsDNA IgG (Fig. S2F), as well as the appearance of anti-RNA IgG (Fig. S2G). Furthermore, IFN-treated KO mice showed monocyte expansion and T cell activation as early as 1 week post-injection (Fig. S2H,I), and two-thirds of these mice died after 35 weeks (Fig. S2J). These results demonstrate that immune activation in KO mice can be accelerated by IFN expression, recapitulating severe SLE in *DNASE1L3*-deficient human patients.

### ***Circulating Dnase1l3 protects from autoreactivity***

We tested the mechanism whereby DNASE1L3 prevents reactivity to self-DNA and SLE. If DNASE1L3 acts similarly to DNASE2 or TREX1 to clear intracellular DNA as proposed (Ghodke-Puranik and Niewold, 2015; Picard et al., 2015), autoreactivity in KO mice should involve the intracellular DNA accumulation and sensing through STING. However, the deletion of STING had no effect on ANA, anti-dsDNA IgG and ASC, splenomegaly and IgG deposition in the kidneys of KO mice (Fig. 3A-E). These data suggest that DNASE1L3 does not target DNA within cells, consistent with the secreted nature of this DNase.

To test the relevance of circulating DNASE1L3, we established an assay based on the digestion of liposome-associated plasmid DNA by mouse serum (Fig. S3A). We then set up reciprocal bone marrow (BM) transfers between WT and KO mice and measured serum DNASE1L3 activity over time. The KO->WT and WT->KO chimeras showed progressive loss and gain of serum DNASE1L3, respectively (Fig. S3B), suggesting that circulating DNASE1L3 is produced by hematopoietic cells. Importantly, the loss of circulating DNASE1L3 in KO->WT chimeras led to the development of anti-dsDNA ASC in the spleen and ANA in the serum (Fig. S3C,D). We analyzed a cohort of fully reconstituted KO->WT chimeras in which DNASE1L3 activity disappeared by 40 weeks post-transfer (Fig. 3F). These mice developed anti-dsDNA IgG starting at the same 40 week time point (Fig. 3G), accompanied by ANA (Fig. 3H), splenomegaly, IgG deposition, glomerular enlargement and mild glomerulonephritis (Fig. S3E,F). Thus, autoreactivity in *Dnase1l3*-deficient mice inversely correlates with circulating DNASE1L3 produced by hematopoietic cells.

To directly test the effect of circulating DNASE1L3 on autoreactivity, we injected young KO mice with an adenoviral vector encoding human DNASE1L3 (Ad-DNASE1L3). Adenoviral vectors *in vivo* transduce hepatocytes and maintain ectopic protein production in them for several weeks, whereupon they are cleared by the immune system. Accordingly, DNASE1L3 activity in the sera of Ad-DNASE1L3-treated KO mice was restored to normal levels at 4 weeks but largely disappeared at 12 weeks post-injection (Fig. 3I). Accordingly, the development of anti-dsDNA IgG titers was transiently but significantly delayed in KO animals treated with Ad-DNASE1L3 compared to the control Ad-GFP (Fig. 3J). Collectively, these results show that circulating DNASE1L3 restricts anti-DNA autoreactivity, likely targeting an extracellular DNA substrate.

### ***Circulating DNASE1L3 is produced by mononuclear phagocytes***

We explored the hematopoietic cell type responsible for the production of circulating DNASE1L3. Microarray expression datasets suggested a restricted expression of *Dnase1l3* primarily in dendritic cells (DC) in both humans and mice (Fig. S4A,B). The predominant expression of *Dnase1l3* in murine conventional DCs (cDCs) was confirmed by qRT-PCR (Fig. S4C). In addition, the expression of *Dnase1l3* was apparent in macrophages (M $\Phi$ ) in select tissues including the spleen, liver and intestine (Fig. S4B). We used the fluorescent detection of LacZ in the targeted *Dnase1l3* allele to confirm the highest expression of *Dnase1l3* in cDC and in a small fraction of splenic M $\Phi$  (Fig. 4A). Consistent with microarray and qRT-PCR data (Fig. S4B,C), low levels of expression were also detected in plasmacytoid DC (pDC), MZB and B-1a cells (Fig. 4A).

Lymphocyte-deficient *Rag1*<sup>-/-</sup> mice had normal levels of serum DNASE1L3, ruling out the contribution of MZB and B-1a cells (Fig. 4B). In contrast, a transient depletion of CD11c<sup>hi</sup> cells (which include all cDC and intestinal MΦ) reduced serum DNASE1L3 by >75% (Fig. 4C). Treatment of WT mice with clodronate liposomes (which deplete tissue MΦ as well as reduce cDC numbers, Fig. S4D) reduced serum DNASE1L3 by ~50% (Fig. 4D). Finally, a single treatment with anti-Csf1r antibody (which primarily depletes intestinal MΦ) reduced serum DNASE1L3 by ~15% (Fig. 4E). Because tissue MΦ are replaced slowly after BM transfer (Hashimoto et al., 2013), the production of DNASE1L3 by MΦ may explain the decline of DNASE1L3 levels in KO->WT chimeras (Fig. 3F). We conclude that circulating DNASE1L3 is produced predominantly by mononuclear phagocytes including cDC and certain tissue MΦ.

### ***DNASE1L3 digests chromatin in apoptotic cell-derived microparticles***

The results above suggested that circulating DNASE1L3 may target an extracellular form of DNA to prevent the activation of DNA-reactive B cells. To identify the relevant DNA target, we examined the ability of recombinant human DNASE1L3 to digest different forms of DNA. As reported previously (Wilber et al., 2002) and confirmed by the analysis of KO mice (Fig. S3A), DNASE1L3 but not DNASE1 could digest liposome-associated plasmid DNA (Fig. 5A,B). In addition, we found that DNASE1L3 was more efficient than DNASE1 in digesting genomic DNA within native polynucleosomes (Fig. 5C). The polymorphic R206C variant of DNASE1L3 maintained its enzymatic activity on all DNA substrates, albeit at reduced level (Fig. 5B,C). In contrast, both specific activities of DNASE1L3, but not the digestion of pure “naked” DNA, were abolished by the deletion of its unique C-terminal peptide (Fig. 5B,C).

Molecular modeling of DNASE1L3 by homology to DNASE1 suggested that the C-terminal peptide comprises a stable  $\alpha$ -helix protruding at a fixed angle from the conserved DNase domain (Fig. S5A-E). Its stable helical conformation together with the net positive charge (9/23 positively charged a.a.) likely facilitates both the membrane binding/penetration and the displacement of DNA from bound histones.

Because microparticles released from apoptotic cells are akin to liposomes and contain nucleosomal DNA (Pisetsky et al., 2010), we hypothesized that this DNA may be a natural substrate of DNASE1L3. Indeed, DNASE1L3 but not DNASE1 digested genomic DNA in microparticles generated from apoptotic Jurkat cells (Fig. 5D) and from apoptotic primary splenocytes (data not shown). Similar to the digestion of liposome-associated and polynucleosomal DNA, the digestion of microparticle DNA was slightly reduced by the R206C polymorphism but completely abolished by the C-terminal deletion. We confirmed the observation (Ullal et al., 2011) that apoptotic microparticles display chromatin on their surface, as revealed by staining with anti-DNA/histone 2a/2b monoclonal antibody (mAb) PR1-3 (Fig. 5E). The PR1-3 staining was insensitive to pre-treatment with DNASE1, consistent with its poor ability to digest intact chromatin. In contrast, the chromatin exposure was abolished by pre-treatment with DNASE1L3, but not by its C-terminal deletion mutant (Fig. 5E). To further dissect the mechanism of DNASE1L3 activity on microparticle DNA, we took advantage of serendipitously generated DNASE1L3 variants with a hexahistidine tag near the C-terminal peptide (Fig. 5A). Whereas the tag at the C-terminus (His-CT) abolished the digestion of both liposome-associated and nucleosomal DNA, the tag preceding the C-terminal peptide (His-preCT) abolished only the digestion of nucleosomal DNA (Fig. 5F). The His-preCT tag is predicted to change the conformation of the C-terminal  $\alpha$ -helical peptide relative

to the DNase domain (Fig. S5E). Importantly, this tag prevented the digestion of DNA within microparticles (Fig. 5F) and on their surface (Fig. 5G), suggesting that the ability to digest nucleosomal DNA is essential for this activity.

We tested whether DNASE1L3 was necessary for the digestion of microparticle DNA in vivo. Serum from KO animals was unable to digest liposome-associated DNA even after the prolonged (60 min.) incubation (Fig. 5H). It was also unable to digest polynucleosomes during a short (15 min) incubation (Fig. 5I). Longer incubation times resulted in complete digestion (Fig. S5F), probably due to the intact serum Dnase1 activity in KO animals. Finally, the serum from KO animals was deficient in the digestion of microparticle DNA (Fig. 5J). Collectively, these data show that DNASE1L3 has two unique and separable activities, i.e. the digestion of liposome-associated DNA and of nucleosomal DNA. These activities enable DNASE1L3 to digest chromatin within and on the surface of apoptotic microparticles, suggesting this DNA form as a natural substrate of DNASE1L3 and a potential antigen in SLE.

### ***DNASE1L3 restricts the amount of DNA in circulating microparticles***

We tested the relationship between DNASE1L3 and the DNA content of microparticles in vivo. Following i.v. injection of Jurkat cell microparticles, their DNA was rapidly cleared from WT mice but persisted up to 24 hours in the serum, spleen and liver of KO mice (Fig. S6A). We then analyzed endogenous microparticles from murine plasma, characterized by their small size, the absence of platelet and erythrocyte markers and positivity for apoptotic marker Annexin V (Fig. S6B). The number of microparticles in the plasma of WT and KO mice was similar (Fig. S6C). However, the amount of genomic DNA in microparticles from KO plasma (measured by PCR for

genomic repeats) was increased >100-fold (Fig. 6A). Accordingly, the amount of DNA in total unfractionated plasma from KO mice was increased >10-fold (Fig. 6B). Furthermore, a fraction of plasma microparticles from young KO animals exposed chromatin on their surface, as revealed by positive staining with PR1-3 (Fig. 6C).

To test whether DNASE1L3 similarly digests circulating microparticle DNA in humans, we analyzed two DNASE1L3-null patients with HUVS (Ozcarar et al., 2013). Neither Patient 1 (HUVS+SLE in remission) nor Patient 2 (HUVS only) had active SLE, ruling out any secondary effects of the disease. Using the digestion of liposome-associated plasmid DNA (Fig. S3B), we confirmed that they had no DNASE1L3 activity in plasma, whereas their haplodeficient parents showed ~50% activity compared to normal subjects (Fig. 6D). We also identified and analyzed three human subjects (one healthy control and two SLE patients) that were heterozygous for the R206C variant of DNASE1L3. These subjects manifested ~60% of control DNASE1L3 activity in plasma (Fig. 6D), suggesting that the R206C variant is ~5-fold less active than the common variant.

Plasma of DNASE1L3-null patients failed to digest nucleosomal DNA (Fig. 6E) as well as microparticle DNA (Fig. 6F), and even the plasma of haplodeficient parents showed detectable impairments in these assays. We then isolated endogenous microparticles from the human plasma in a manner similar to murine microparticles, and confirmed previous reports (Nielsen et al., 2011) that Annexin V<sup>+</sup> microparticles express markers of leukocytes and include a granulocyte marker-positive fraction (Fig. S6D). Microparticles from DNASE1L3-null patients carried >1000-fold more DNA than those from healthy controls, and microparticles from haplodeficient parents or R206C carriers also showed an increased DNA content (Fig. 6G). The analysis of human plasma

samples showed that nearly all detectable genomic DNA is contained within the microparticle fraction (Fig. S6E). Accordingly, total unfractionated plasma of DNASE1L3-null patients also harbored increased amounts of circulating DNA (Fig. 6H). Collectively, genetic evidence in animals and humans demonstrates that DNASE1L3 digests genomic DNA circulating in plasma, specifically within apoptotic cell-derived microparticles.

### ***DNASE1L3 prevents the recognition of microparticle DNA by autoantibodies***

We tested whether DNA within microparticles, and specifically the DNASE1L3-sensitive chromatin on their surface, is targeted by autoantibodies in experimental SLE. Sera from KO but not WT mice contained IgG binding to Jurkat microparticles (Fig. 7A), and this reactivity was prominent in all examined KO mice starting from a young age (Fig. 7B). The KO IgG also bound to microparticles from splenocytes, albeit less efficiently (data not shown). The binding was abolished by pre-treatment of microparticles with DNASE1L3 (Fig. 7C), confirming that it is directed towards DNASE1L3-sensitive chromatin on their surface. Similar DNASE1L3-sensitive binding was also displayed by several anti-DNA/anti-nucleosome mAbs from mouse SLE models (Fig. S7A), including the prototypic 3H9 mAb (Shlomchik et al., 1987). To directly test whether microparticles can elicit anti-DNA responses, we injected wild-type animals with microparticles generated from syngeneic apoptotic splenocytes. Consecutive i.v. injections of microparticles failed to elicit anti-dsDNA or anti-chromatin response in naïve animals (Fig. 7D and data not shown). However, microparticle injections into animals treated with the IFN adenovirus induced high titers of anti-

nucleosome IgG (Fig. 7D). Thus, in the context of infection and/or IFN response, microparticles can represent antigens that elicit chromatin-specific B cell responses.

Finally, we asked whether DNASE1L3-sensitive chromatin in microparticles is recognized by autoantibodies in human SLE. The *DNASE1L3*-deficient Patient 1 (HUVS+SLE in remission) harbored IgG binding to microparticles in a DNASE1L3-sensitive manner (Fig. 7E). Neither the *DNASE1L3*-deficient Patient 2 (HUVS without SLE) nor the healthy *DNASE1L3*-haplodeficient parents manifested IgG binding to microparticles (Fig. 7E). Human IgG carrying the 9G4 idiotope are prominent among SLE-associated autoantibodies and bind multiple antigens including DNA, cell nuclei and apoptotic cell surface determinants (Jenks et al., 2013; Richardson et al., 2013). Among several 9G4<sup>+</sup> mAb clones from SLE patients, two (75G15 and 74C2) showed DNASE1L3-sensitive binding to microparticles (Fig. S7B); notably, these two clones are among the strongest binders to apoptotic cell membranes (Richardson et al., 2013). Finally, we tested whether DNASE1L3-sensitive chromatin on microparticles represents an antigen in patients with sporadic SLE. None of healthy control subjects (n=10) but 64% of SLE patients (n=53) harbored IgG binding to microparticles (Fig. S7C and 7F,G). The binding to microparticles showed a weak but significant correlation with anti-dsDNA titers (data not shown), as observed for IgG binding to endogenous microparticles in SLE (Ullal et al., 2011). Importantly, the binding was sensitive to DNASE1L3 pre-treatment in ~36% of patients (Fig. S7D and 7F,G), suggesting that it is directed against chromatin components on the surface of microparticles. Collectively, our data in mice and humans suggest that chromatin on circulating apoptotic microparticles is an antigen for DNA-reactive B cells and antibodies produced by them.

This chromatin is a physiological substrate for circulating DNASE1L3, which limits its availability and may thereby protect from anti-DNA reactivity and SLE.

## Discussion

SLE in *DNASE1L3*-deficient human patients is characterized by early onset, absence of a sex bias and the presence of anti-dsDNA IgG (Al-Mayouf et al., 2011; Ozcakar et al., 2013). We found that these features were recapitulated in *Dnase1l3*-deficient mice, all of which develop anti-dsDNA reactivity on two distinct genetic backgrounds. Hereditary SLE has been difficult to model in mice: for instance, null mutations in the complement component *C1Q* or in the nucleotide-processing enzyme *SAMHD1* cause SLE in human patients (Ghodke-Puranik and Niewold, 2015; Picard et al., 2015) but no overt pathology in mice (Heidari et al., 2006; Rehwinkel et al., 2013). Given that the hypomorphic DNASE1L3 variant is associated with non-familial SLE, our mouse model should also be relevant for common forms of the disease. Furthermore, the robust autoimmunity in the absence of *Dnase1l3* contrasts with *Dnase1*-deficient mice, in which infrequent and late autoantibody development was described only on a mixed genetic background (Napirei et al., 2000). Therefore, our results confirm DNASE1L3 as an essential, evolutionarily conserved mediator of tolerance to DNA.

Circulating IgG to dsDNA began developing as early as 5 weeks of age in *Dnase1l3*-deficient mice. This reactivity may comprise a part of a broader response to chromatin, which developed concomitantly and preceded anti-dsDNA in many animals. In contrast, the reactivity to other self-antigens was either absent (e.g. RNA) or developed much later (e.g. extracellular matrix components). Similarly, except for the expansion of monocytes, all classical signs of immune activation (splenomegaly, GC

reaction, T cell activation) appeared only in old animals. This delay likely reflects the lack of additional disease-promoting mutations common in SLE models, such as those causing lymphoproliferation (e.g. *Fas*<sup>lpr</sup>) or heightened RNA sensing (e.g. *Yaa*). Another important aspect is the paucity of immune stimulation in specific pathogen-free mice, as opposed to human patients who are constantly exposed to infections. Indeed, the treatment with IFN induced anti-RNA response, accelerated immune activation and caused significant mortality. These data suggest that the reactivity to nucleosomal DNA within chromatin causes all subsequent pathological features, and in conjunction with a strong inflammatory stimulus can yield a severe SLE-like disease.

Ablation of cytoplasmic DNA sensing by the deletion of STING abolishes inflammatory disease caused by DNASE2 or TREX1 deficiency (Ahn et al., 2012; Gall et al., 2012); conversely, it exacerbates autoimmunity in polygenic or chemically induced models by increasing responsiveness to TLR ligands (Sharma et al., 2015). In contrast, the deletion of STING had no effect on anti-DNA responses or the ensuing disease in *Dnase1/3*-deficient mice. The endosomal DNA sensor TLR9 was similarly dispensable (data not shown), consistent with its complex and often protective roles in other models (Green and Marshak-Rothstein, 2011; Shlomchik, 2009). Accordingly, no signs of activation or developmental abnormalities could be detected in DCs or B cells from young *Dnase1/3*-null mice (Fig. 2 and data not shown). These data suggest that the primary anti-DNA antibody response may be largely independent of innate DNA sensing, and instead results from a direct antigen receptor-mediated expansion of DNA-reactive B cells. Given the absence of grossly elevated GC responses in young mice, such B cells are likely to undergo extrafollicular activation and class switching. Thus, the

mechanism of anti-DNA reactivity in *Dnase1/3*-deficient mice likely reflects the primary loss of antigen-specific B cell tolerance to DNA.

Similar to its homolog DNASE1, DNASE1L3 is a secreted enzyme that is present in systemic circulation (Napirei et al., 2009), as confirmed in our study. Importantly, the levels of circulating DNASE1L3 inversely correlated with the development of anti-dsDNA antibodies in BM chimeras and in the mice reconstituted with secreted DNASE1L3. Combined with the dispensability of STING-mediated intracellular DNA sensing, these observations strongly suggest that DNASE1L3 acts in a cell-extrinsic manner to shield autoreactive B cells from antigenic self-DNA. Notably, we found that *Dnase1/3* is expressed specifically in DCs and select tissue macrophages, which appear to produce the bulk of secreted DNASE1L3. These observations strongly support the important role of mononuclear phagocytes such as DCs and macrophages in self-tolerance and restriction of autoimmunity (Ganguly et al., 2013; Lavin et al., 2015). Such tolerogenic function has been associated primarily with tissue-specific phagocytic activity (e.g. engulfment of apoptotic cells), induction of T cell tolerance and expression of anti-inflammatory cytokines and surface molecules by the phagocytes. Our work describes an entirely different mechanism of tolerogenic activity by these cells, whereby their secretion of a DNA-processing enzyme enforces global B cell tolerance to DNA.

Our data show that DNASE1L3 i) acts systemically in a cell-extrinsic manner; ii) has a unique capacity to digest membrane-associated DNA; iii) has a preferential capacity to digest DNA within nucleosomes. All these properties point to the chromatin within circulating microparticles as the physiological substrate of DNASE1L3, as confirmed by genetic evidence from *DNASE1L3*-deficient animals and human subjects.

DNA-containing microparticles are normally present in the human plasma (Dieker et al., 2016; Nielsen et al., 2011; Nielsen et al., 2012) and appear to be derived from cells that die within the vessel lumen. In particular, surface staining ((Nielsen et al., 2011) and this study) suggests that some microparticles are derived from myeloid cells, consistent with the ultra-rapid turnover of circulating granulocytes. The DNA in microparticles is cell-extrinsic yet not soluble, and therefore would be digested neither by cell-intrinsic DNases (e.g. DNase2) nor by common secreted DNases (e.g. DNase1). Notably, we found that the majority of genomic DNA detectable in human plasma was contained within the microparticle fraction. Indeed, total human plasma DNA was shown to be derived primarily from leukocytes and to comprise nucleosomal fragments of chromatin (Holdenrieder et al., 2005; Rumore and Steinman, 1990; Snyder et al., 2016; Sun et al., 2015). Accordingly, DNASE1L3 deficiency increased the DNA load of circulating microparticles, as well as the total amount of DNA in plasma. Although other potential DNA substrates of DNASE1L3 cannot be ruled out, these data strongly implicate microparticle-associated DNA as the relevant endogenous target of DNASE1L3.

A striking feature of chromatin in apoptotic blebs and circulating microparticles is its exposure at the membrane surface and accessibility to autoantibodies (Casciola-Rosen et al., 1994; Cocca et al., 2002; Radic et al., 2004; Ullal et al., 2011). The same chromatin would necessarily be accessible to the antigen receptor of DNA-reactive B cells, comprising an antigenic DNA form for humoral anti-DNA responses. We found that exposed chromatin on microparticles is digested by DNASE1L3, and becomes a target of autoantibodies in *Dnase1/3*-deficient animals and in the *DNASE1L3*-deficient human patient with SLE history. Importantly, DNASE1L3-sensitive chromatin on the surface of microparticles appears to be targeted by prototypic autoreactive clones from

murine and human SLE, as well as by serum IgG from at least one third of patients with sporadic SLE. The latter is consistent with the reported binding of IgG and complement to plasma microparticles in human SLE patients (Nielsen et al., 2012; Ullal et al., 2011). Therefore, irrespective of genetic DNASE1L3 deficiency, microparticle-associated chromatin may represent a common antigenic form of self-DNA in SLE.

In conclusion, we here identify chromatin in microparticles as a latent self-antigen for autoreactive B cells, and circulating DNASE1L3 as an essential factor that restricts its antigenicity and prevents anti-DNA responses. These results provide a mechanistic explanation for the association of null and hypomorphic DNASE1L3 mutations with familial and sporadic SLE, respectively. They also uncover a cell-extrinsic mechanism of tolerance to DNA that involves a secreted enzyme and therefore can be developed for therapeutic purposes. In particular, the observed delay of anti-DNA reactivity by DNASE1L3 re-expression warrants the exploration of DNASE1L3 protein delivery as a therapeutic tool in SLE and other systemic autoimmune diseases.

## **Experimental Procedures**

**Animals.** All experiments were performed according to the investigator's protocol approved by the Institutional Animal Care and Use Committees of Columbia University and New York University. Mice with a targeted germline replacement of *Dnase1l3* (*Dnase1l3<sup>LacZ</sup>*) have been purchased from Taconic Knockout Repository (model TF2732), backcrossed onto 129SvEvTac or C57BL/6 backgrounds for >10 generations and intercrossed to obtain *Dnase1l3<sup>LacZ/LacZ</sup>* knockout animals. Age-matched wild-type mice of the respective backgrounds were bred in the same animal colony and used as controls. STING-deficient mice (C57BL/6J-*Tmem173<sup>gt</sup>*/J, Jackson

Laboratories) were crossed with *Dnase1/3<sup>LacZ</sup>* mice and backcrossed to obtain double-deficient animals on C57BL/6 background. Hematopoietic reconstitution and cell depletion experiments are described in Supplemental Procedures.

**Human subjects.** *DNASE1L3*-deficient HUVS patients 1 and 2 correspond to patients IV-4 and IV-5 from Family 1 described in (Ozcakar et al., 2013). Their study was approved by the Ethics Committees of Ankara University (Turkey) and by the IRB at the University of Miami (U.S.A), and informed consents were obtained from the parents. Blood from patients with sporadic SLE and healthy controls was obtained from the NYU IRB-approved Rheumatology SAMPLE (Specimen and Matched Phenotype Linked Evaluation) Biorepository. All patients signed an IRB-approved informed consent. All subjects were genotyped for *DNASE1L3 rs35677470* using the TaqMan assay (ThermoFisher), and three subjects (one healthy control and two SLE patients) were found heterozygous for the rare allele encoding *DNASE1L3 R206C*. Additional information is provided in Supplemental Procedures.

**Adenoviruses.** Adenoviral vector encoding *IFN $\alpha$ 5* (Mathian et al., 2005) was kindly provided by A. Davidson (Feinstein Institute for Medical Research). Adenoviral vector encoding human *DNASE1L3* was constructed by Welgen, Inc. Adenoviral particles were produced and purified at Welgen, Inc., and were injected into the indicated mice i.v. at  $0.5-1 \times 10^{10}$  particles per mouse.

**Analysis of autoreactivity.** Flow cytometry, immunochemistry, ANA, ELISA, ELISPOT, antigen arrays and the analysis of kidney IgG deposition and histopathology are described in Supplemental Procedures.

**Recombinant DNases.** Cloned ORF of human *DNASE1* and *DNASE1L3* (NCBI accession NP\_004935.1) were subcloned into pMCSV-IRES-GFP (pMIG) retroviral

expression vector. The constructs for DNASE1L3 variants were generated using the Q5 site-directed mutagenesis kit (NEB) and included the R206->C substitution; the C-terminal truncation (a.a. 282-305); and the insertions of hexahistidine between a.a. 282-283 (His-preCT) or between a.a. 305 and the stop codon (His-CT). The resulting constructs or the empty pMIG were used as plasmids for the transient transfection of HEK293 cells using the TransIT-293 reagent (Mirus Bio), and equal efficiency of transfection was confirmed by flow cytometry for GFP expression. To avoid contamination with DNases in bovine serum, transfection was performed in medium with 15% KnockOUT serum supplement (Thermo Fisher). Transfected cells were cultured for 48 hr and the supernatants were collected, filtered and stored in aliquots. Prior to freezing, 4 mM CaCl<sub>2</sub> and 4 mM MgCl<sub>2</sub> were added to yield a final concentration of 2 mM in DNase activity assays.

**Analysis of DNASE1L3 activity.** To measure the digestion of liposome-associated DNA, pMIG plasmid DNA was pre-incubated with DOTAP (Roche) according to the manufacturer's instructions in HBSS. Native or DOTAP-coated plasmid (1 ng/reaction) was incubated with an equal volume of DNase-containing supernatants or sera for 60 min at 37°C in a total reaction volume of 2 µl. The amount of remaining DNA was measured by qPCR with GFP-specific primers and expressed as % of input DNA using a calibration curve with serial plasmid dilutions. For the measurement of relative DNASE1L3 activity in vivo, the digestion was performed for 10 min using 1 µl of mouse serum or human serum or plasma in a final volume of 5 µl. After qPCR, the amount of remaining DNA was converted to % of DNASE1L3 activity using a calibration curve with serial dilutions of control wild-type serum or plasma used to digest coated DNA in the same conditions.

To measure the digestion of nucleosomal DNA, we used purified human polynucleosomes from HeLa cells (Epiccypher). Polynucleosomes (2 ng/reaction) were incubated with an equal volume of Dnase-containing supernatants for 15 min at 37°C in a total reaction volume of 2  $\mu$ l. The amount of remaining DNA was measured by qPCR with primers specific for human genomic *Alu* repeats and expressed as % of input DNA using a calibration curve with serial polynucleosomes dilutions.

**Generation and administration of microparticles.** Microparticles from Jurkat cells were generated as previously described (Ullal et al., 2011). Briefly, the cells were cultured in the presence of 1 mM staurosporine (Sigma-Aldrich) overnight, harvested and collected by centrifugation for 5 min at 1500 rpm. The supernatants were collected and centrifuged at 22000 *g* for 30 min to pellet the microparticles, which were analyzed on the Accuri C6 flow cytometer (BD Biosciences) to determine absolute numbers and ensure >95% enrichment. Where indicated, microparticles ( $10^5/\mu$ l in PBS) were incubated with an equal volume of DNase-containing transfection supernatants for 1 hr at 37°C.

Primary mouse splenocytes were cultured for 2-3 days with 50 ng/ml phorbol 12-myristate 13-acetate (PMA) and 2  $\mu$ g/mL ionomycin (Sigma-Aldrich). The resulting cultures of activated splenocytes were treated with staurosporine overnight and used to purify microparticles as above. To administer microparticles in vivo, wild-type female 129 mice were injected with PBS or with the IFN $\alpha$ 5 adenovirus ( $5 \times 10^9$  viral particles). One week later, the mice were injected i.v. with  $10^7$  microparticles in 100  $\mu$ l PBS generated as above from wild-type 129 splenocytes. The injection was repeated total of four times at weekly intervals, and the mice were analyzed one week after the last injection.

**Isolation of circulating microparticles.** To isolate microparticles from human plasma, blood was collected in tubes containing EDTA, and blood cells were removed by centrifugation at 2000 *g* for 10 minutes at 4°C. In some experiments, a second centrifugation step (3,000 *g* for 10 minutes) was used to remove platelets as described (Nielsen et al., 2011). The resulting plasma (either fresh or stored at -80°C) was centrifuged at 22,000 *g* for 30-60 min to pellet the microparticles, and the supernatant was used to measure DNASE1L3 activity and antibody binding specificities. To isolate microparticles from murine plasma, animals were euthanized and immediately exsanguinated by cardiac puncture into heparin-containing tubes. Plasma was isolated by centrifugation at 2000 *g* for 10 minutes 4°C and centrifuged at 22,000 *g* for 30 min to pellet the microparticles. Microparticles were resuspended and counted by flow cytometry after staining for CD42b and CD235a (human) or CD41 and Ter119 (mouse) to exclude platelets and erythrocytes.

**Analysis of microparticles.** To test the ability of mouse serum or human plasma to digest microparticle DNA, Jurkat microparticles ( $5 \times 10^5/\mu\text{l}$  in PBS) were incubated with an equal volume of serum/plasma for 1 hr at 37°C in a final reaction volume of 10  $\mu\text{l}$ . The DNA content of Jurkat cell-derived microparticles, human plasma microparticles and total plasma was measured by qPCR for human genomic *Alu* repeats. The DNA content of murine plasma microparticles and total plasma was measured by qPCR for mouse genomic *B1* repeats. Data were converted into the amount of genomic DNA using calibration curves with the respective genomic DNA, and expressed as % of input DNA or as amount of DNA per microparticle.

For surface staining,  $2.5 \times 10^5$  native or DNase-treated Jurkat cell microparticles were stained with either purified anti-DNA/histone 2a/2b mAb PR1-3 (10  $\mu\text{g}/\text{ml}$ ) or

mouse sera (1:10 dilution) for 30 minutes at 4°C. Stained microparticles were washed by centrifugation at 22000 g for 30 min, incubated with PE-labeled goat anti–mouse IgG secondary antibody (eBioscience) at a 1:200 dilution for 30 minutes at 4°C and analyzed by flow cytometry without further washing. Staining with human sera or plasma was done as above at 1:20 dilution, using PE-labeled goat anti–human IgG secondary antibody (eBioscience).

**Statistics.** To allow robust statistical analysis, we did not assume normal distribution of values (Weissgerber et al., 2015). Unless indicated otherwise, the data were displayed as medians with range of individual values and their significance was estimated by nonparametric Mann-Whitney test.

### **Acknowledgements**

We thank G. Silverman for help and discussions, M. Shlomchik and A. Davidson for reagents and S. Rasmussen for technical assistance. Supported by NIH grants AR064460 and AI072571 and the Lupus Research Institute (B.R.), The Judith and Stewart Colton Center for Autoimmunity (B.R. and J.P.B.) and the Irvington Institute Fellowship of the Cancer Research Institute (V.S.).

## References

- Ahn, J., Gutman, D., Saijo, S., and Barber, G.N. (2012). STING manifests self DNA-dependent inflammatory disease. *Proc Natl Acad Sci U S A* 109, 19386-19391.
- Al-Mayouf, S.M., Sunker, A., Abdwani, R., Arawi, S.A., Almurshedi, F., Alhashmi, N., Al Sonbul, A., Sewairi, W., Qari, A., Abdallah, E., *et al.* (2011). Loss-of-function variant in DNASE1L3 causes a familial form of systemic lupus erythematosus. *Nat Genet* 43, 1186-1188.
- Baron, W.F., Pan, C.Q., Spencer, S.A., Ryan, A.M., Lazarus, R.A., and Baker, K.P. (1998). Cloning and characterization of an actin-resistant DNase I-like endonuclease secreted by macrophages. *Gene* 215, 291-301.
- Bizzaro, N., Villalta, D., Giavarina, D., and Tozzoli, R. (2012). Are anti-nucleosome antibodies a better diagnostic marker than anti-dsDNA antibodies for systemic lupus erythematosus? A systematic review and a study of metanalysis. *Autoimmun Rev* 12, 97-106.
- Campbell, A.M., Kashgarian, M., and Shlomchik, M.J. (2012). NADPH oxidase inhibits the pathogenesis of systemic lupus erythematosus. *Sci Transl Med* 4, 157ra141.
- Casciola-Rosen, L.A., Anhalt, G., and Rosen, A. (1994). Autoantigens targeted in systemic lupus erythematosus are clustered in two populations of surface structures on apoptotic keratinocytes. *J Exp Med* 179, 1317-1330.
- Choi, J., Kim, S.T., and Craft, J. (2012). The pathogenesis of systemic lupus erythematosus-an update. *Curr Opin Immunol* 24, 651-657.
- Cocca, B.A., Cline, A.M., and Radic, M.Z. (2002). Blebs and apoptotic bodies are B cell autoantigens. *J Immunol* 169, 159-166.
- Crow, Y.J. (2015). Type I interferonopathies: mendelian type I interferon up-regulation. *Curr Opin Immunol* 32, 7-12.
- Dieker, J., Tel, J., Pieterse, E., Thielen, A., Rother, N., Bakker, M., Franssen, J., Dijkman, H.B., Berden, J.H., de Vries, J.M., *et al.* (2016). Circulating Apoptotic Microparticles in Systemic Lupus Erythematosus Patients Drive the Activation of Dendritic Cell Subsets and Prime Neutrophils for NETosis. *Arthritis & rheumatology* 68, 462-472.
- Ehlers, M., Fukuyama, H., McGaha, T.L., Aderem, A., and Ravetch, J.V. (2006). TLR9/MyD88 signaling is required for class switching to pathogenic IgG2a and 2b autoantibodies in SLE. *J Exp Med* 203, 553-561.
- Elkon, K.B., and Wiedeman, A. (2012). Type I IFN system in the development and manifestations of SLE. *Curr Opin Rheumatol* 24, 499-505.
- Fairhurst, A.M., Wandstrat, A.E., and Wakeland, E.K. (2006). Systemic lupus erythematosus: multiple immunological phenotypes in a complex genetic disease. *Adv Immunol* 92, 1-69.
- Gall, A., Treuting, P., Elkon, K.B., Loo, Y.M., Gale, M., Jr., Barber, G.N., and Stetson, D.B. (2012). Autoimmunity initiates in nonhematopoietic cells and progresses via lymphocytes in an interferon-dependent autoimmune disease. *Immunity* 36, 120-131.
- Ganguly, D., Haak, S., Sisirak, V., and Reizis, B. (2013). The role of dendritic cells in autoimmunity. *Nat Rev Immunol* 13, 566-577.
- Garcia-Romo, G.S., Caielli, S., Vega, B., Connolly, J., Allantaz, F., Xu, Z., Punaro, M., Baisch, J., Guiducci, C., Coffman, R.L., *et al.* (2011). Netting neutrophils are

- major inducers of type I IFN production in pediatric systemic lupus erythematosus. *Sci Transl Med* 3, 73ra20.
- Ghodke-Puranik, Y., and Niewold, T.B. (2015). Immunogenetics of systemic lupus erythematosus: A comprehensive review. *J Autoimmun* 64, 125-136.
- Green, N.M., and Marshak-Rothstein, A. (2011). Toll-like receptor driven B cell activation in the induction of systemic autoimmunity. *Semin Immunol* 23, 106-112.
- Hashimoto, D., Chow, A., Noizat, C., Teo, P., Beasley, M.B., Leboeuf, M., Becker, C.D., See, P., Price, J., Lucas, D., *et al.* (2013). Tissue-resident macrophages self-maintain locally throughout adult life with minimal contribution from circulating monocytes. *Immunity* 38, 792-804.
- Heidari, Y., Bygrave, A.E., Rigby, R.J., Rose, K.L., Walport, M.J., Cook, H.T., Vyse, T.J., and Botto, M. (2006). Identification of chromosome intervals from 129 and C57BL/6 mouse strains linked to the development of systemic lupus erythematosus. *Genes Immun* 7, 592-599.
- Holdenrieder, S., Stieber, P., Chan, L.Y., Geiger, S., Kremer, A., Nagel, D., and Lo, Y.M. (2005). Cell-free DNA in serum and plasma: comparison of ELISA and quantitative PCR. *Clinical chemistry* 51, 1544-1546.
- Jenks, S.A., Palmer, E.M., Marin, E.Y., Hartson, L., Chida, A.S., Richardson, C., and Sanz, I. (2013). 9G4+ autoantibodies are an important source of apoptotic cell reactivity associated with high levels of disease activity in systemic lupus erythematosus. *Arthritis Rheum* 65, 3165-3175.
- Lande, R., Ganguly, D., Facchinetti, V., Frasca, L., Conrad, C., Gregorio, J., Meller, S., Chamilos, G., Sebasigari, R., Ricciari, V., *et al.* (2011). Neutrophils activate plasmacytoid dendritic cells by releasing self-DNA-peptide complexes in systemic lupus erythematosus. *Sci Transl Med* 3, 73ra19.
- Lavin, Y., Mortha, A., Rahman, A., and Merad, M. (2015). Regulation of macrophage development and function in peripheral tissues. *Nat Rev Immunol* 15, 731-744.
- Lood, C., Blanco, L.P., Purmalek, M.M., Carmona-Rivera, C., De Ravin, S.S., Smith, C.K., Malech, H.L., Ledbetter, J.A., Elkon, K.B., and Kaplan, M.J. (2016). Neutrophil extracellular traps enriched in oxidized mitochondrial DNA are interferogenic and contribute to lupus-like disease. *Nature medicine* 22, 146-153.
- Mathian, A., Weinberg, A., Gallegos, M., Banchereau, J., and Koutouzov, S. (2005). IFN-alpha induces early lethal lupus in preautoimmune (New Zealand Black x New Zealand White) F1 but not in BALB/c mice. *J Immunol* 174, 2499-2506.
- Mayes, M.D., Bossini-Castillo, L., Gorlova, O., Martin, J.E., Zhou, X., Chen, W.V., Assassi, S., Ying, J., Tan, F.K., Arnett, F.C., *et al.* (2014). ImmunoChip analysis identifies multiple susceptibility loci for systemic sclerosis. *Am J Hum Genet* 94, 47-61.
- Mizuta, R., Araki, S., Furukawa, M., Furukawa, Y., Ebara, S., Shiokawa, D., Hayashi, K., Tanuma, S., and Kitamura, D. (2013). DNase gamma is the effector endonuclease for internucleosomal DNA fragmentation in necrosis. *PloS one* 8, e80223.
- Nagata, S., and Kawane, K. (2011). Autoinflammation by endogenous DNA. *Adv Immunol* 110, 139-161.
- Napirei, M., Karsunky, H., Zevnik, B., Stephan, H., Mannherz, H.G., and Moroy, T. (2000). Features of systemic lupus erythematosus in Dnase1-deficient mice. *Nat Genet* 25, 177-181.

- Napirei, M., Ludwig, S., Mezrhab, J., Klockl, T., and Mannherz, H.G. (2009). Murine serum nucleases--contrasting effects of plasmin and heparin on the activities of DNase1 and DNase1-like 3 (DNase113). *FEBS J* 276, 1059-1073.
- Napirei, M., Wulf, S., Eulitz, D., Mannherz, H.G., and Klockl, T. (2005). Comparative characterization of rat deoxyribonuclease 1 (Dnase1) and murine deoxyribonuclease 1-like 3 (Dnase113). *Biochem J* 389, 355-364.
- Nielsen, C.T., Ostergaard, O., Johnsen, C., Jacobsen, S., and Heegaard, N.H. (2011). Distinct features of circulating microparticles and their relationship to clinical manifestations in systemic lupus erythematosus. *Arthritis Rheum* 63, 3067-3077.
- Nielsen, C.T., Ostergaard, O., Stener, L., Iversen, L.V., Truedsson, L., Gullstrand, B., Jacobsen, S., and Heegaard, N.H. (2012). Increased IgG on cell-derived plasma microparticles in systemic lupus erythematosus is associated with autoantibodies and complement activation. *Arthritis Rheum* 64, 1227-1236.
- Ozcakar, Z.B., Foster, J., 2nd, Diaz-Horta, O., Kasapcopur, O., Fan, Y.S., Yalcinkaya, F., and Tekin, M. (2013). DNASE1L3 mutations in hypocomplementemic urticarial vasculitis syndrome. *Arthritis Rheum* 65, 2183-2189.
- Picard, C., Mathieu, A.L., Hasan, U., Henry, T., Jamilloux, Y., Walzer, T., and Belot, A. (2015). Inherited anomalies of innate immune receptors in pediatric-onset inflammatory diseases. *Autoimmun Rev* 14, 1147-1153.
- Pisetsky, D.S. (2016). Anti-DNA antibodies - quintessential biomarkers of SLE. *Nat Rev Rheumatol* 12, 102-110.
- Pisetsky, D.S., Gauley, J., and Ullal, A.J. (2010). Microparticles as a source of extracellular DNA. *Immunol Res* 49, 227-234.
- Radic, M., Marion, T., and Monestier, M. (2004). Nucleosomes are exposed at the cell surface in apoptosis. *J Immunol* 172, 6692-6700.
- Rehwinkel, J., Maelfait, J., Bridgeman, A., Rigby, R., Hayward, B., Liberatore, R.A., Bieniasz, P.D., Towers, G.J., Moita, L.F., Crow, Y.J., *et al.* (2013). SAMHD1-dependent retroviral control and escape in mice. *EMBO J* 32, 2454-2462.
- Rekvig, O.P., van der Vlag, J., and Seredkina, N. (2014). Review: antinucleosome antibodies: a critical reflection on their specificities and diagnostic impact. *Arthritis & rheumatology* 66, 1061-1069.
- Richardson, C., Chida, A.S., Adlowitz, D., Silver, L., Fox, E., Jenks, S.A., Palmer, E., Wang, Y., Heimburg-Molinaro, J., Li, Q.Z., *et al.* (2013). Molecular basis of 9G4 B cell autoreactivity in human systemic lupus erythematosus. *J Immunol* 191, 4926-4939.
- Rumore, P.M., and Steinman, C.R. (1990). Endogenous circulating DNA in systemic lupus erythematosus. Occurrence as multimeric complexes bound to histone. *The Journal of clinical investigation* 86, 69-74.
- Sang, A., Zheng, Y.Y., and Morel, L. (2013). Contributions of B cells to lupus pathogenesis. *Mol Immunol*.
- Santiago-Raber, M.L., Amano, H., Amano, E., Baudino, L., Otani, M., Lin, Q., Nimmerjahn, F., Verbeek, J.S., Ravetch, J.V., Takasaki, Y., *et al.* (2009). Fcγ receptor-dependent expansion of a hyperactive monocyte subset in lupus-prone mice. *Arthritis Rheum* 60, 2408-2417.
- Sharma, S., Campbell, A.M., Chan, J., Schattgen, S.A., Orłowski, G.M., Nayar, R., Huyler, A.H., Nundel, K., Mohan, C., Berg, L.J., *et al.* (2015). Suppression of systemic autoimmunity by the innate immune adaptor STING. *Proc Natl Acad Sci U S A* 112, E710-717.

- Shiokawa, D., and Tanuma, S. (2001). Characterization of human DNase I family endonucleases and activation of DNase gamma during apoptosis. *Biochemistry* 40, 143-152.
- Shlomchik, M.J. (2009). Activating systemic autoimmunity: B's, T's, and tolls. *Curr Opin Immunol* 21, 626-633.
- Shlomchik, M.J., Aucoin, A.H., Pisetsky, D.S., and Weigert, M.G. (1987). Structure and function of anti-DNA autoantibodies derived from a single autoimmune mouse. *Proc Natl Acad Sci U S A* 84, 9150-9154.
- Snyder, M.W., Kircher, M., Hill, A.J., Daza, R.M., and Shendure, J. (2016). Cell-free DNA Comprises an In Vivo Nucleosome Footprint that Informs Its Tissues-Of-Origin. *Cell* 164, 57-68.
- Sun, K., Jiang, P., Chan, K.C., Wong, J., Cheng, Y.K., Liang, R.H., Chan, W.K., Ma, E.S., Chan, S.L., Cheng, S.H., *et al.* (2015). Plasma DNA tissue mapping by genome-wide methylation sequencing for noninvasive prenatal, cancer, and transplantation assessments. *Proc Natl Acad Sci U S A* 112, E5503-5512.
- Ueki, M., Takeshita, H., Fujihara, J., Iida, R., Yuasa, I., Kato, H., Panduro, A., Nakajima, T., Kominato, Y., and Yasuda, T. (2009). Caucasian-specific allele in non-synonymous single nucleotide polymorphisms of the gene encoding deoxyribonuclease I-like 3, potentially relevant to autoimmunity, produces an inactive enzyme. *Clin Chim Acta* 407, 20-24.
- Ullal, A.J., Marion, T.N., and Pisetsky, D.S. (2014). The role of antigen specificity in the binding of murine monoclonal anti-DNA antibodies to microparticles from apoptotic cells. *Clin Immunol* 154, 178-187.
- Ullal, A.J., Reich, C.F., 3rd, Clowse, M., Criscione-Schreiber, L.G., Tochacek, M., Monestier, M., and Pisetsky, D.S. (2011). Microparticles as antigenic targets of antibodies to DNA and nucleosomes in systemic lupus erythematosus. *J Autoimmun* 36, 173-180.
- Volkman, H.E., and Stetson, D.B. (2014). The enemy within: endogenous retroelements and autoimmune disease. *Nat Immunol* 15, 415-422.
- Wardemann, H., and Nussenzweig, M.C. (2007). B-cell self-tolerance in humans. *Adv Immunol* 95, 83-110.
- Weissgerber, T.L., Milic, N.M., Winham, S.J., and Garovic, V.D. (2015). Beyond bar and line graphs: time for a new data presentation paradigm. *PLoS Biol* 13, e1002128.
- Wilber, A., Lu, M., and Schneider, M.C. (2002). Deoxyribonuclease I-like III is an inducible macrophage barrier to liposomal transfection. *Mol Ther* 6, 35-42.
- Zochling, J., Newell, F., Charlesworth, J.C., Leo, P., Stankovich, J., Cortes, A., Zhou, Y., Stevens, W., Sahhar, J., Roddy, J., *et al.* (2014). An Immunochip-based interrogation of scleroderma susceptibility variants identifies a novel association at DNASE1L3. *Arthritis Res Ther* 16, 438.

## Figure legends

### Figure 1. *Dnase1/3*-deficient mice rapidly develop antibodies to double-stranded DNA and chromatin.

(A) Anti-nuclear antibodies (ANA) in the sera of *Dnase1/3*-deficient knockout (KO) and control wild-type (WT) mice. Shown are fixed Hep2 cells incubated with sera from 50-week-old mice on 129 or B6 backgrounds, followed by staining for IgG (red) and DNA (blue). Representative of 6 independent animals in each group (scale bars, 50  $\mu\text{m}$  and in the inset 20  $\mu\text{m}$ ).

(B) Serum titers of anti-dsDNA IgG in WT or KO mice on the indicated backgrounds as determined by ELISA. Shown are titers from individual animals (circles) and median titers (bars) at the indicated time points.

(C) Serum titers of anti-dsDNA IgG subclasses in 40-week-old KO mice on the 129 background as measured by ELISA.

(D-E) Anti-dsDNA IgG antibody-secreting cells (ASC) in WT and KO mice as determined by ELISPOT. Shown are ASC numbers per  $5 \times 10^5$  splenocytes in 50 week old (D) and 4-6 week old (E) mice of the indicated backgrounds.

(F) Serum titers of anti-nucleosome IgG in WT or KO mice on the 129 background as determined by ELISA. Data are shown as in panel B.

(G-H) Relative titers of anti-dsDNA and anti-nucleosome IgG in a synchronous cohort of KO mice analyzed over time. Titers are presented as % of the maximal value reached at any time point in each individual mice. Shown is the kinetics in three representative individual mice (panel G) and values in individual mice at 5 weeks (panel H). Significance was estimated by paired Wilcoxon test.

Statistical significance is indicated as follows: \*,  $P \leq 0.05$ ; \*\*,  $P \leq 0.01$ ; \*\*\*,  $P \leq 0.001$ .

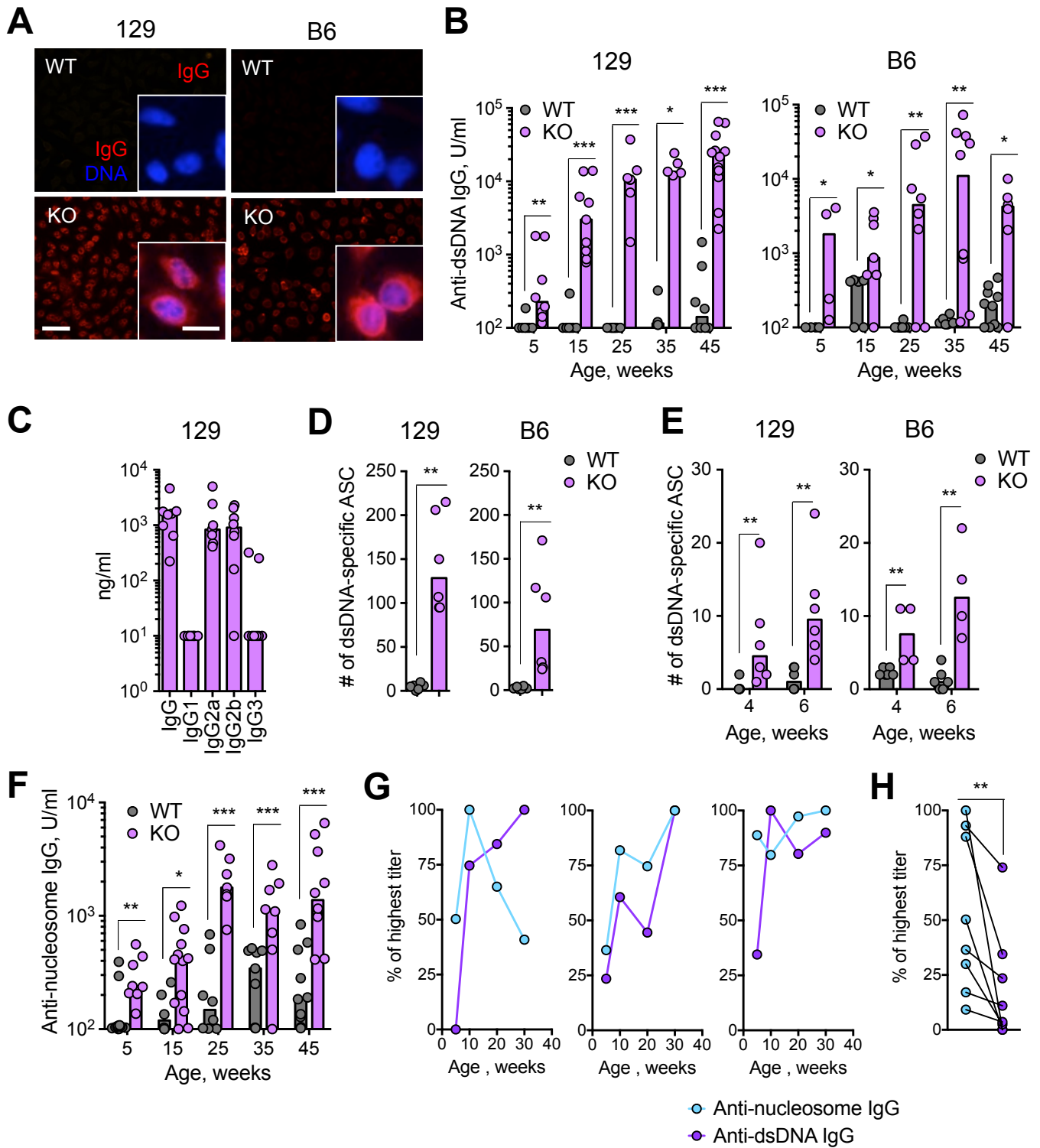


**Fig. 1**

**Figure 2. *Dnase1/3*-deficient mice develop late-onset immune activation and kidney inflammation.**

(A-B) Monocyte population in the peripheral blood of *Dnase1/3*-deficient knockout (KO) and control wild-type (WT) mice. Panel A shows representative staining of peripheral blood mononuclear cells (PBMC) from WT and KO mice, with the fraction and phenotype of CD11c<sup>+</sup> MHC cl. II<sup>-</sup> monocytes indicated. Panel B shows fractions of CD11c<sup>+</sup> MHC cl. II<sup>-</sup> monocytes among PBMC at the indicated time points (median ± interquartile range of 9 animals per group).

(C) Representative spleens from WT and KO mice on a 129 background at 50 weeks of age.

(D) Absolute number of splenocytes in WT or KO mice at the indicated time points. Shown are values from individual animals (circles); bars indicate the median.

(E) The GC B cell population in the spleens of WT or KO mice at the indicated time points. Shown are the fractions of GC B cells (B220<sup>+</sup> PNA<sup>+</sup> CD95<sup>+</sup>) among total B220<sup>+</sup> B cells as determined by flow cytometry.

(F) The GC reaction in the spleens of WT or KO mice at 50 weeks of age. Shown are splenic sections stained by immunofluorescence for total B cells (B220, red) and GC B cells (PNA, green; scale bar 200 μm) with the individual GC in the inset (scale bar 20 μm). Representative of 6 mice per genotype.

(G) IgG deposition in the kidneys of WT or KO mice at 50 weeks of age. Shown are kidney sections stained by immunofluorescence for IgG (red) and DNA (blue). Representative of 10 animals per group (scale bar, 50 μm).

(H) Kidney architecture in WT or KO mice on a 129 background at 50 weeks of age. Shown are kidney sections stained with hematoxylin/eosin (scale bars, 50 μm) with a representative glomerulus in the inset. Representative of 8 animals per group.

(I) Histopathological score of glomerulonephritis in WT or KO mice at 50 weeks of age. Shown is the percentage of kidney cortex affected by inflammation and the median cumulative score of glomerulonephritis in mice on the indicated backgrounds.

Statistical significance is indicated as follows: \*,  $P \leq 0.05$ ; \*\*,  $P \leq 0.01$ ; \*\*\*,  $P \leq 0.001$ .

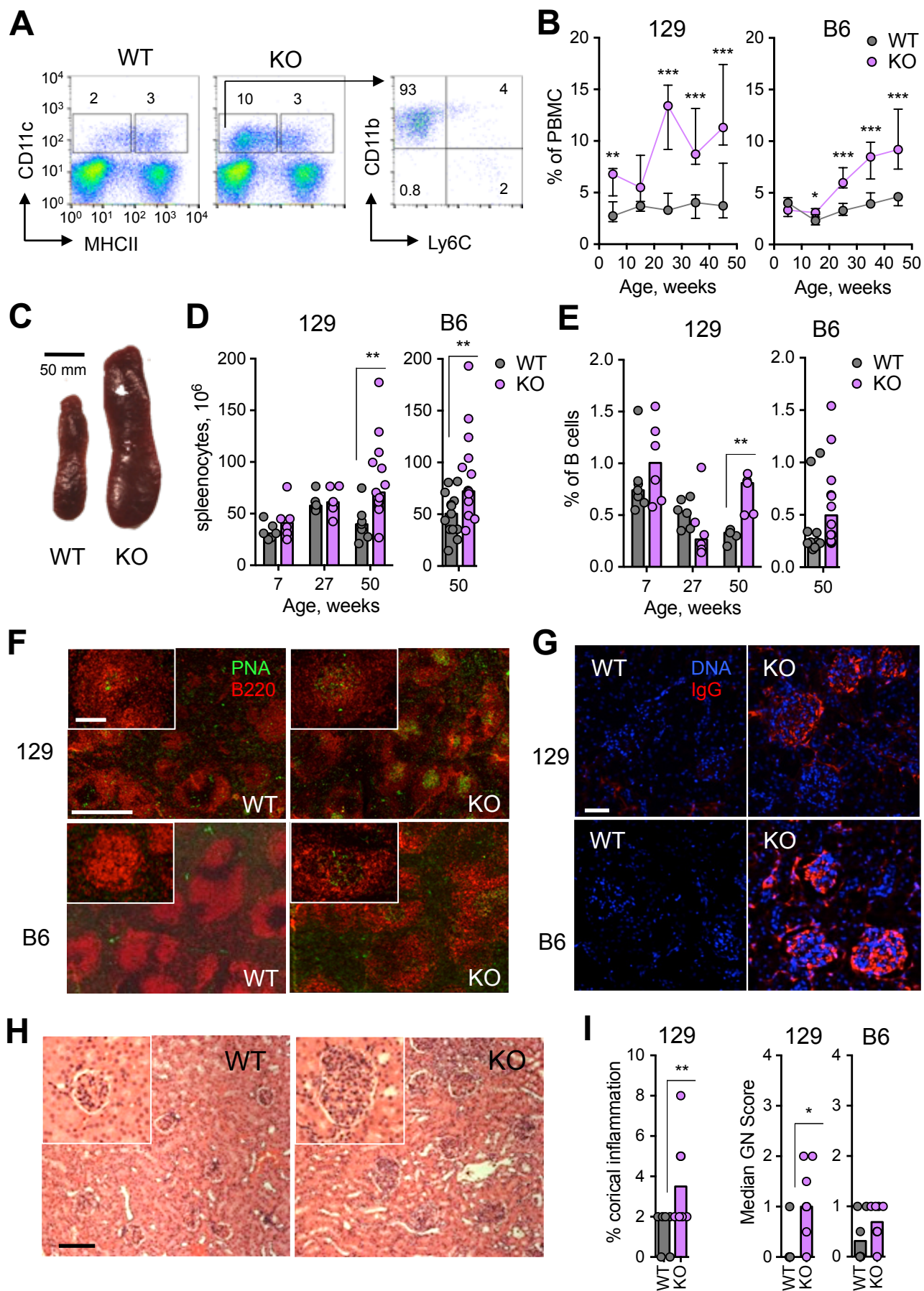


**Fig. 2**

**Figure 3. Autoreactivity in *Dnase1/3*-deficient mice does not require STING and is restricted by circulating DNASE1L3**

*Dnase1/3*-deficient knockout (KO) mice were crossed with STING-deficient mice to generate double-KO (dKO) mice on the B6 background, and analyzed along with respective wild-type (WT) controls.

(A) Serum ANA at 45 weeks of age. Results are shown as in Fig. 1A; representative of 6 animals per group.

(B) Serum titers of anti-dsDNA IgG at 35 weeks of age as determined by ELISA.

(C) Anti-dsDNA IgG antibody-secreting cells (ASC) at 50 weeks of age as determined by ELISPOT. Shown are numbers of ASC per  $5 \times 10^5$  splenocytes.

(D) Splenic weight at 50 weeks of age.

(E) IgG deposition in the kidneys at 50 weeks of age. Results are shown as in Fig. 2G; representative of 5 animals per group (scale bar, 50  $\mu$ m).

(F-H) WT recipients were lethally irradiated and reconstituted with WT or KO BM, KO-to-WT and control WT-to-WT chimeras, respectively.

(F) Serum Dnase1L3 activity in chimeras at the indicated time points after reconstitution (mean  $\pm$  SD of 6 animals per group).

(G) Serum anti-dsDNA IgG titers at the indicated time points as measured by ELISA.

(H) ANA in the sera of chimeras at 50 weeks post-reconstitution.

(I-J) Autoreactivity in KO mice reconstituted with circulating DNASE1L3. Young 4 week old KO mice were injected with adenoviruses encoding DNASE1L3 (Ad-DNASE1L3) or GFP (Ad-GFP).

(F) Serum Dnase1L3 activity in KO mice administered Ad-DNASE1L3 or Ad-GFP at the indicated time points, along with age-matched wild-type controls.

(G) Serum anti-dsDNA IgG titers in KO mice administered Ad-DNASE1L3 or Ad-GFP as measured by ELISA (median  $\pm$  range of 4 (WT and KO + Ad-GP) and 9 (KO + Ad-DNASE1L3) animals per group)

Statistical significance is indicated as follows: \*,  $P \leq 0.05$ ; \*\*,  $P \leq 0.01$ ; \*\*\*,  $P \leq 0.001$ .

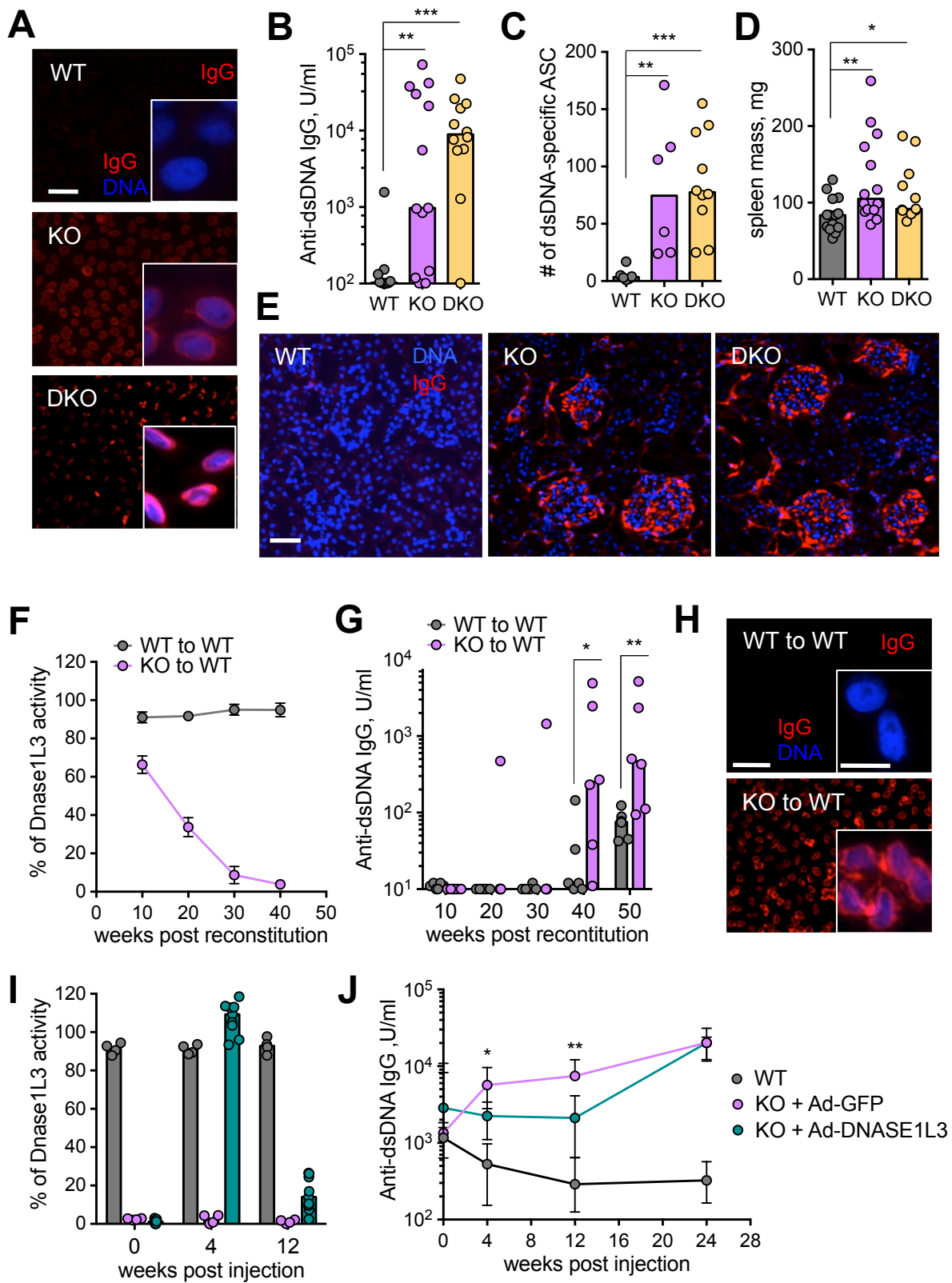


**Fig. 3**

**Figure 4. Circulating DNASE1L3 is produced primarily by dendritic cells and macrophages.**

(A) Single-cell analysis of Dnase1L3 expression in immune cells. Splenocytes from *Dnase1l3*<sup>LacZ/LacZ</sup> KO or WT control mice were stained for LacZ activity using the fluorescent  $\beta$ -galactosidase substrate FDG and analyzed by flow cytometry. Shown are histograms of FDG staining in the indicated gated cell populations (representative of 3 independent experiments). Similar results were obtained with heterozygous *Dnase1l3*<sup>LacZ/+</sup> mice (not shown).

(B) Dnase1L3 activity in the sera of Rag1-deficient animals.

(C) Dnase1L3 activity in the sera of DC-depleted animals. Animals with Cre-inducible diphtheria toxin receptor (DTR) with or without the DC-specific Cre deleter (CD11c-Cre) were administered diphtheria toxin (DTX) for 2 weeks, and their sera was analyzed for DNASE1L3 activity.

(D) Dnase1L3 activity in the sera of wild-type animals treated with PBS- or clodronate-containing liposomes to deplete macrophages on the indicated days after treatment.

(E) Dnase1L3 activity in the sera of wild-type animals 12 days after injection of control IgG or anti-Csf1r blocking antibody.

Statistical significance is indicated as follows: \*,  $P \leq 0.05$ ; \*\*,  $P \leq 0.01$ ; \*\*\*,  $P \leq 0.001$ .

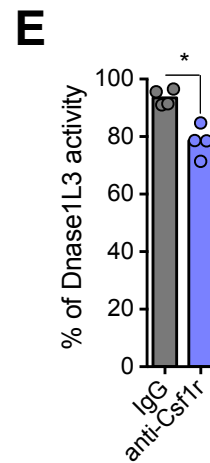
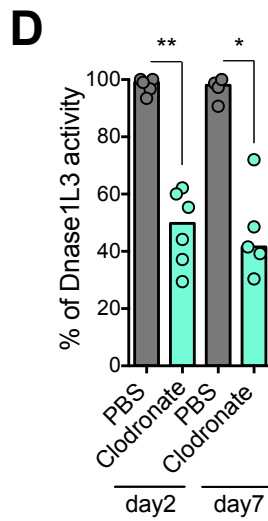
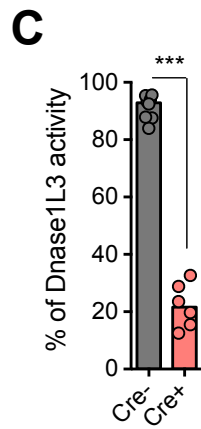
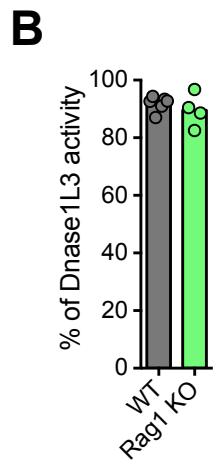
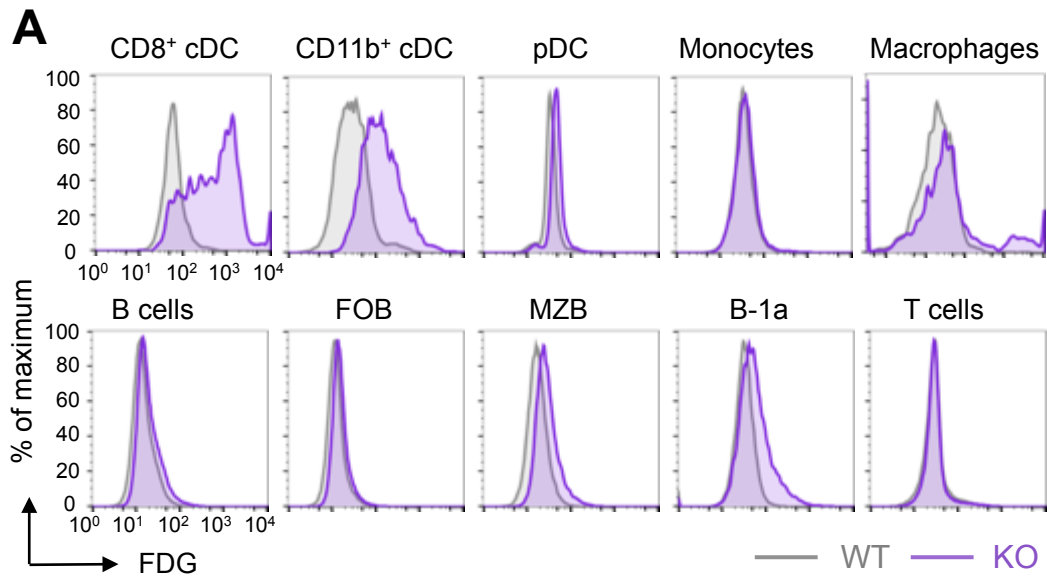


**Fig. 4**

**Figure 5. DNASE1L3 can digest intact chromatin and genomic DNA in apoptotic microparticles**

(A) Schematic of different DNase constructs used.

(B-D) Digestion of different DNA substrates by recombinant DNases. DNA substrates were incubated with a control supernatant (empty, grey) or supernatants containing DNASE1, DNASE1L3, its C-terminal truncation (DNASE1L3  $\Delta$ CT) or its R206C substitution variant. The amount of remaining DNA was measured by qPCR and expressed as % of input DNA (mean  $\pm$  SD of 3 independent experiments).

(B) The digestion of plasmid DNA alone (DNA) or in complex with liposomal reagent (DNA DOTAP)

(C) The digestion of purified human genomic DNA (gDNA) or purified human nucleosomes (nDNA).

(D) The digestion of DNA within microparticles from apoptotic human cells (MP DNA).

(E) The digestion of chromatin on the surface of microparticles by recombinant DNases. Microparticles from apoptotic human cells were incubated with DNase-containing supernatants described above and stained with anti-nucleosome mAb PR1-3. Shown are histograms of PR1-3 fluorescence and the % of positive MP; representative of 3 experiments.

(F) Digestion of DNA substrates by DNASE1L3 mutants with a hexahistidine tag at the C-terminus (His-CT) or preceding it (His-preCT). DNA substrates and data presentation are as in panels B-D.

(G) The digestion of chromatin on the surface of microparticles by hexahistidine-containing DNASE1L3 mutants. Data are presented as in panel E.

(H-J) Digestion of different DNA substrates by sera from *Dnase1l3*-deficient knockout (KO) or control wild-type (WT) animals. The digestion of plasmid DNA with or without DOTAP (panel H), human purified or nucleosomal genomic DNA (panel I) or DNA within microparticles from apoptotic human cells (panel J) was measured as in panels B-D. Shown are results from sera of individual animals (circles) and median (lines). Statistical significance is indicated as follows: \*\*,  $P \leq 0.01$ ; \*\*\*,  $P \leq 0.001$ .

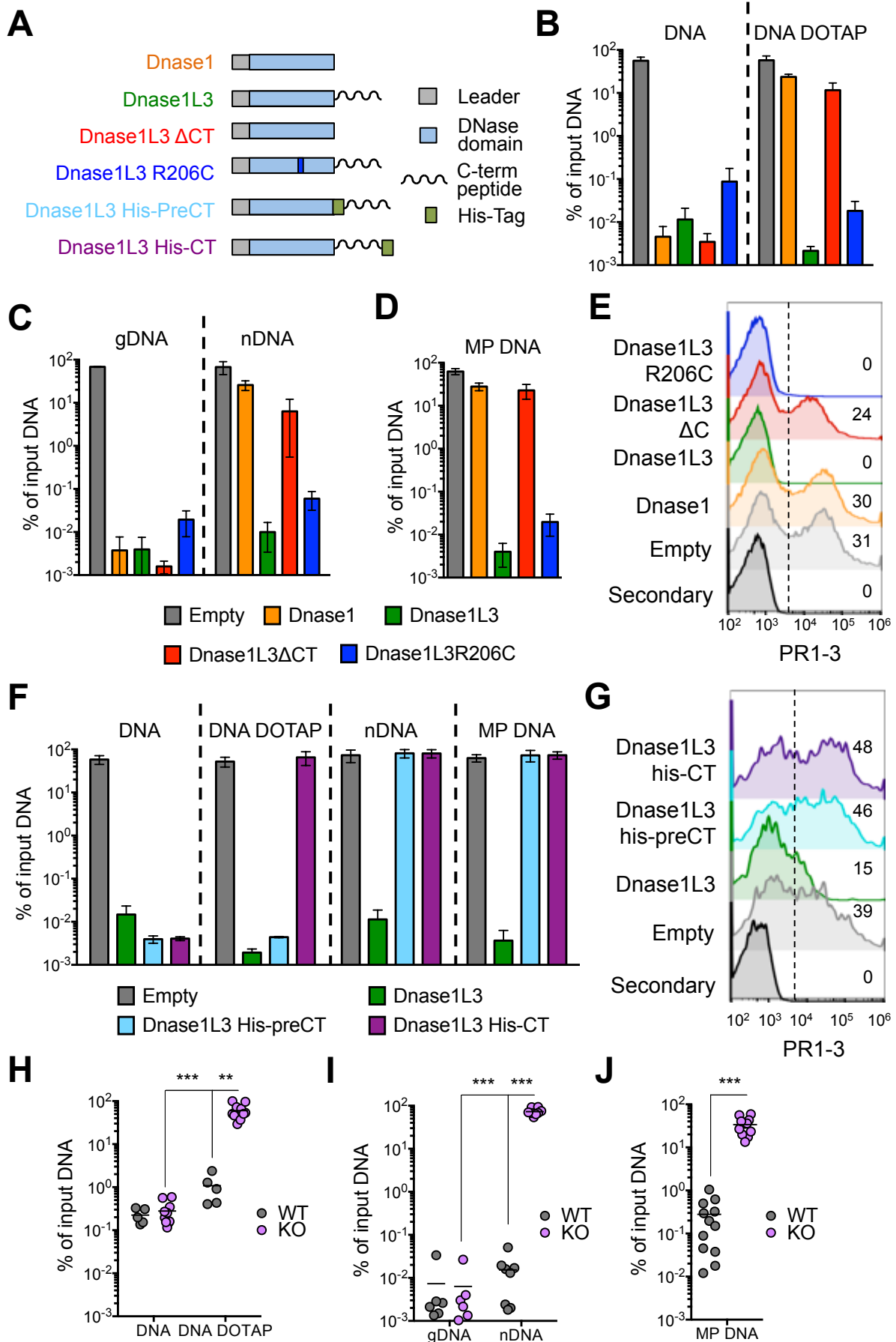


**Fig. 5**

**Figure 6. DNASE1L3 deficiency in mice and human patients causes the accumulation of DNA in circulating microparticles**

(A) The genomic DNA cargo of circulating microparticles (MP) from *Dnase1l3*-deficient knockout (KO) or control wild-type (WT) animals. MP were isolated from the plasma of 10 week old mice and analyzed by qPCR for mouse genomic DNA. Results show the amount of DNA per MP in individual mice (circles) and group median (bar).

(B) The amount of genomic DNA per volume of unfractionated plasma from WT and KO animals as determined by qPCR.

(C) The binding of anti-nucleosome mAb PR1-3 to circulating microparticles isolated from the plasma of young KO or WT mice. Shown are representative histograms of PR1-3 fluorescence and the frequency of positive MP after staining MP from individual mice.

(D-H) Plasma from human *DNASE1L3*-deficient patients (n=2), their haplodeficient parents (n=2), individuals with the *DNASE1L3* R206C polymorphism (n=3) and normal control subjects (n=2-5) were analyzed.

(D) *DNASE1L3* activity in the soluble fraction of patients' plasma, measured using the digestion of DOTAP-coated plasmid DNA and expressed as a % of activity in a reference control plasma.

(E) The digestion of human nucleosomes by the soluble fraction of patients' plasma.

(F) The digestion of DNA in microparticles from apoptotic human cells by the soluble fraction of patients' plasma.

(G) The amount of genomic DNA in circulating microparticles (MP) isolated from the plasma. Results show the amount of DNA per MP as determined by qPCR for human genomic DNA.

(H) The amount of genomic DNA per volume of unfractionated plasma as determined by qPCR.

Statistical significance is indicated as follows: \*\*,  $P \leq 0.01$ ; \*\*\*,  $P \leq 0.001$ .

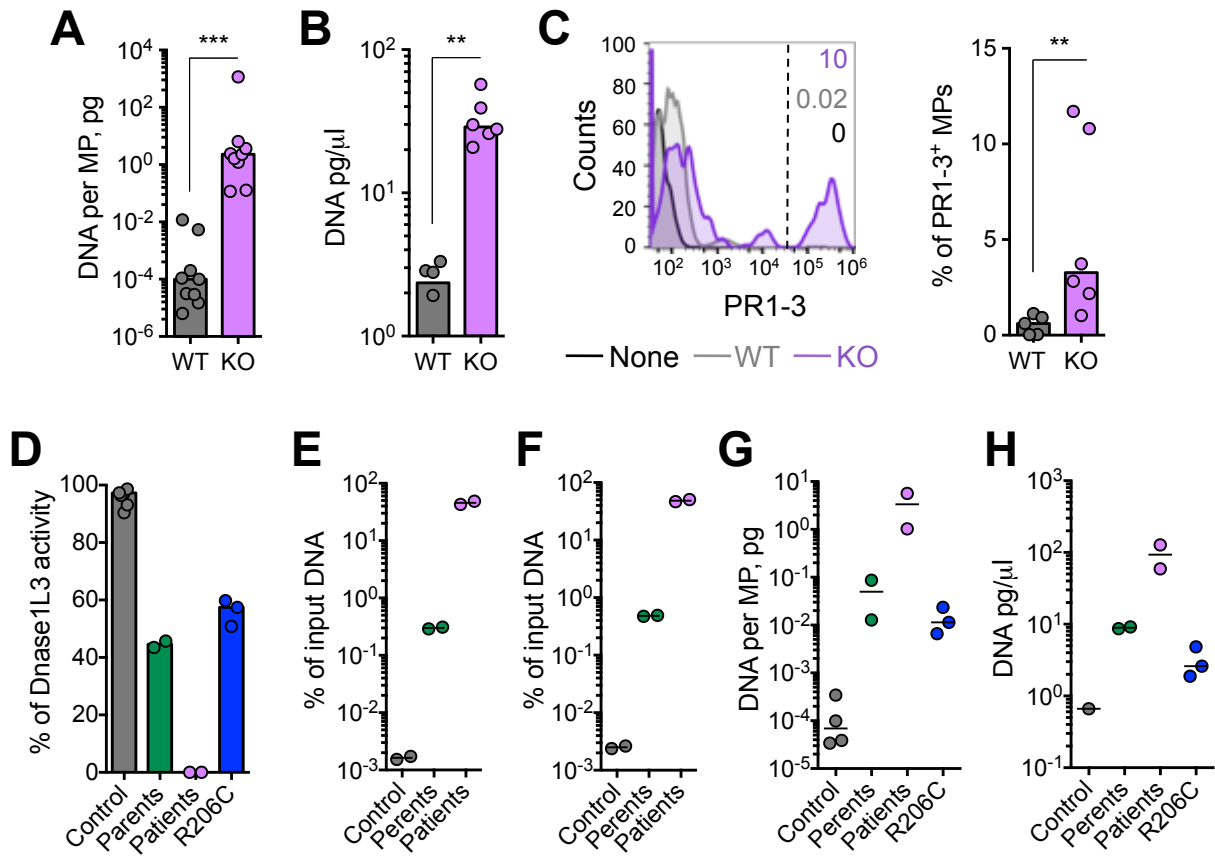


Fig. 6

**Figure 7. DNASE1L3-sensitive chromatin on apoptotic microparticles is antigenic in mice and human patients**

(A-C) Binding of mouse serum IgG to the surface of microparticles (MP). Human apoptotic MP were incubated with sera from *Dnase1/3*-deficient knockout (KO) or control wild-type (WT) animals, followed by secondary anti-mouse IgG antibody.

(A) Representative histograms of IgG fluorescence and the % of positive MP.

(B) Fractions of IgG-positive MP stained with sera from WT or KO mice of the indicated ages (median  $\pm$  range of 5 animals per group)

(C) MP were incubated with supernatants containing human DNASE1 or DNASE1L3 or an empty control prior to the staining with KO serum. Shown are representative histograms of IgG fluorescence and the frequency of positive MP stained by sera from 5 individual KO mice.

Statistical significance is indicated as follows: \*,  $P \leq 0.05$ ; \*\*,  $P \leq 0.01$ ; \*\*\*,  $P \leq 0.001$ .

(D) Anti-nucleosome response in the animals immunized with microparticles. Wild-type mice were administered IFN $\alpha$  adenovirus (IFN), microparticles from syngeneic apoptotic splenocytes (MP) or both, and serum IgG to nucleosomes were measured by ELISA one week after the last MP immunization. Shown are titers from individual animals (circles) and median titers (bars).

(E-G) DNASE1L3-sensitive binding of IgG from human patients to the surface of microparticles. Human apoptotic MP were treated with DNASE1L3-containing supernatant (DNASE1L3) or a control supernatant (empty), incubated with plasma from human subjects, followed by secondary anti-human IgG antibody. Shown are representative histograms of IgG fluorescence and the % of positive MP.

(E) DNASE1L3-sensitive binding of IgG from *DNASE1L3*-deficient patients or their haplodeficient parents. Shown are representative histograms of IgG fluorescence and the % of positive MP.

(F) DNASE1L3-sensitive binding of IgG from patients with sporadic SLE. Shown are two representative histograms of IgG fluorescence for each reactivity pattern.

(G) The fraction of SLE patients with the reactivity patterns shown in panel F.

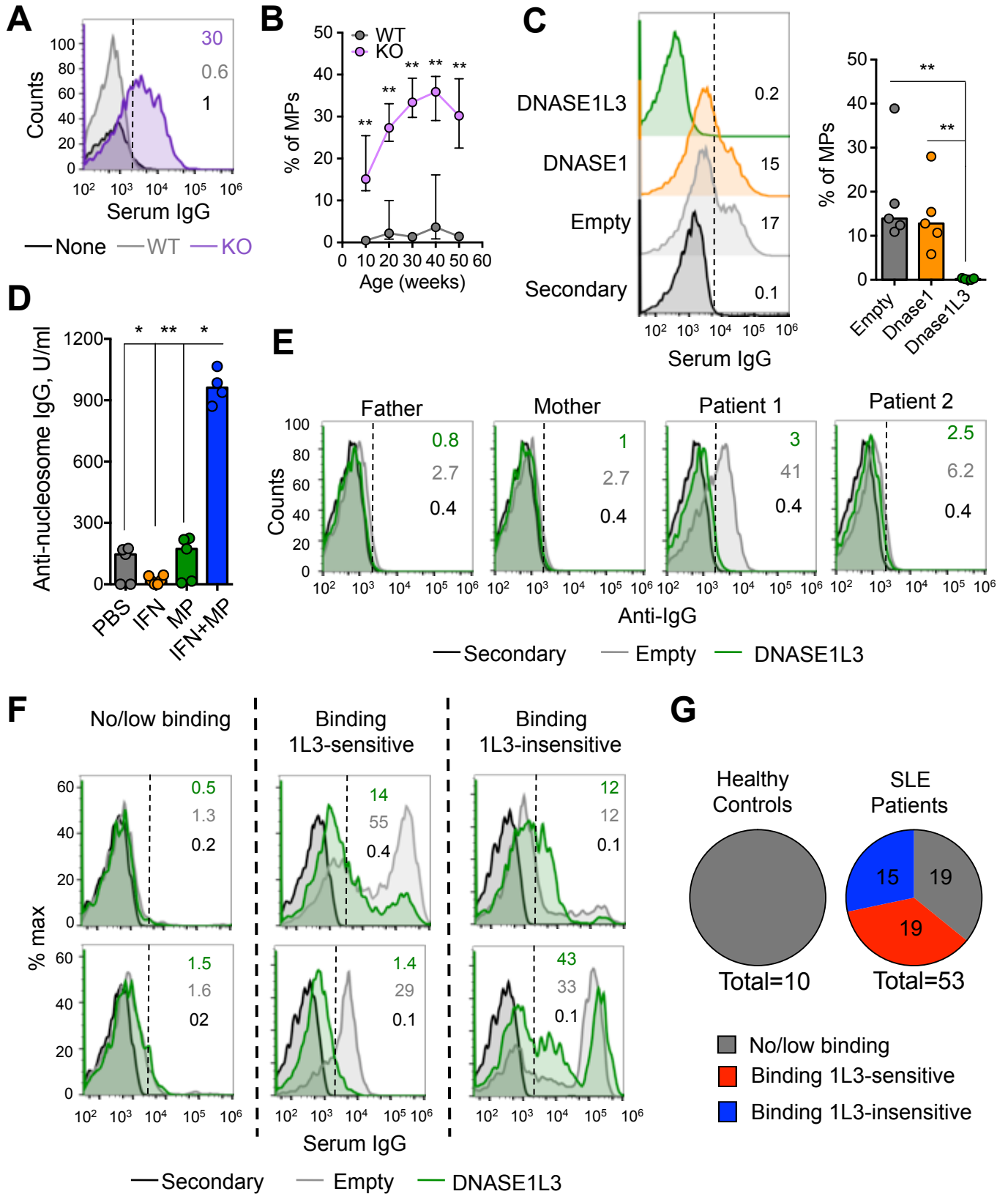


**Fig. 7**

## Supplemental Experimental Procedures

**Human subjects.** DNASE1L3-deficient patients 1 and 2 correspond to patients IV-4 and IV-5 from Family 1 described in (Ozcarar et al., 2013). Patient 1 (14 y.o. female) developed SLE with ANA and high anti-dsDNA 6 years ago. She was treated with rituximab (last dose in May 2012) and has been in clinical remission since then (weak ANA, normal anti-dsDNA), except for active uveitis. Patient 2 (12 y.o. female) has no SLE (negative ANA and anti-dsDNA) but ongoing active HUVS with severe vasculitis of the kidney. All patients with sporadic SLE met  $\geq 4$  revised American College of Rheumatology criteria (Hochberg, 1997), and 28/53 (53%) of them had anti-dsDNA at the time of analysis.

**Hematopoietic reconstitution.** For the experiment in Fig. S3B-D, total BM cells ( $2 \times 10^6$ ) from WT or KO mice on the 129 background were transferred into lethally irradiated WT and KO recipients on the B6 background, which has the same MHC haplotype. Reconstitution was determined by staining for the 129 donor strain-specific CD229.1 leukocyte marker. For the experiment in Fig. 3F-H and S3E-F, BM cells from WT or KO mice on the (129xB6)F1 background were transferred into the congenic (129xB6.SJL)F1 recipients. Reconstitution was determined by staining for the B6.SJL recipient strain-specific CD45.1 leukocyte marker. Donor contribution was  $>95\%$  in all analyzed chimeras.

**Cell depletions.** *Rag1*-deficient mice were obtained from Jackson Laboratories. For dendritic cell (DC) depletion, animals with Cre-inducible diphtheria toxin receptor (iDTR) allele (Buch et al., 2005) were crossed with the DC-specific Cre deleter strain *CD11c*-Cre (Caton et al., 2007). The resulting *CD11c*-Cre/iDTR mice were administered diphtheria toxin (DTX) 20 ng/g every second day for 2 weeks as described (Yogev et al., 2012), yielding efficient DC depletion. For macrophage depletion with anti-Csf1r, B6 mice were injected i.p. with 150  $\mu\text{g/g}$  of body weight Csf1r-blocking antibody (clone AFS98, (Sudo et al., 1995)) purified from a hybridoma as described previously (Hashimoto et al., 2011). For macrophage depletion with clodronate, mice were injected i.v. with a single dose (200  $\mu\text{l}$ ) of clodronate liposomes (5 mg/ml) or control PBS liposomes (obtained from ClodronateLiposomes.com).

***In vivo* persistence of microparticles.** Jurkat cell-derived microparticles were injected i.v. at  $6 \times 10^6$  per mouse into wild-type mice. The recipient mice were euthanized at indicated time points and their tissues were analyzed by qPCR for human DNA.

**ELISA.** Anti-dsDNA, anti-RNA and anti-chondroitin IgG titers were determined by ELISA as previously described (Blanco et al., 1991; Giltiay et al., 2013) using plates pre-coated with poly-L-lysine (0.05 mg/ml) for 2 hr at room temperature and then coated with with 0.1 mg/ml calf thymus DNA, yeast RNA or chondroitin sulfates A from bovine trachea (Sigma-Aldrich) as antigens. Anti-nucleosome IgG titers were determined using plates pre-coated with 1  $\mu$ g/ml of purified Hela polynucleosomes (Epicpher) as antigen. After incubation with sera, the amount of bound IgG was measured with an AP-conjugated goat anti-mouse IgG antibody (1:5000, Jackson ImmunoResearch). Antigen-specific IgG titers were determined using serial dilution of the serum from a positive animal as a standard, and expressed as units per volume. Anti-dsDNA IgG isotypes were measured by ELISA using calf thymus DNA as antigen and alkaline phosphatase (AP)-conjugated antibodies to IgG isotypes (Southern Biotech). Total immunoglobulin levels in the serum were determined by ELISA using AP-conjugated antibodies to IgM, IgA, IgG, and IgG isotypes (Southern Biotech).

**ELISPOT.** To detect antibody-secreting cells (ASC) specific to dsDNA, 96-well multiscreen plates (Millipore) were pre-treated for 1 min with 35% ethanol, coated with calf thymus dsDNA (100  $\mu$ g/ml, Sigma-Aldrich, washed and blocked with 3% FCS 3% BSA in PBS. Single-cell suspensions of total splenocytes were plated in duplicates in six two-fold serial dilutions starting at  $10^6$  cells/well and incubated for 5 hr at 37°C. The plates were washed and incubated with AP-conjugated goat anti-mouse IgG (1:5000, Jackson ImmunoResearch) overnight at 4°C. Spots were developed using NBT/BCIT (Sigma-Aldrich) system and counted using ImmunoSpot Series 1 ELISPOT analyzer (Cellular Technology Ltd).

**Anti-nuclear antibodies (ANA).** Fixed HEp-2 cells (MBL Bion) were incubated with mouse serum (1:100 dilution) followed by PE-labeled goat anti-mouse IgG and DAPI. Images were captured on a confocal fluorescent microscope (LSM 710 NLO) and processed by Zen software (Carl Zeiss).

**Antigen Array.** A total of 35 lupus-associated autoantigens were spotted in replicates of 6 on SuperEpoxy 2 slides (TeleChem) as described (Quintana et al., 2004;

Wu et al., 2008). The microarrays were blocked with 1% bovine serum albumin and incubated for 2 hr at 37°C with the test serum diluted 1:200 in blocking buffer. The arrays were then washed and incubated for 45 min with a 1:500 dilution of goat anti-mouse IgG or IgM Cy3-conjugated detection antibodies (Jackson ImmunoResearch) using a Tecan HS4800 Pro hybridization station (Tecan). The arrays were scanned with a Tecan PowerScanner (Tecan). Raw data were normalized and analyzed using the GeneSpring software (Silicon Genetics). Antigen reactivity was defined by the mean intensity of binding to the replicates of that antigen on the microarray, and expressed as relative fluorescence units (RFU). Pairwise comparison of the samples was done using the NIA Array software (Sharov et al., 2005).

**IgG deposition.** Both kidneys were fixed in 4% paraformaldehyde, dehydrated in 30% sucrose and frozen in OCT (TissueTek). Frozen sections (5 µm) were stained with DAPI and PE-labeled goat anti-mouse IgG (eBioscience) and visualized by microscopy as above.

**Spleen immunohistochemistry.** To visualize the GC reaction, frozen spleen sections (5 µm) were stained with PE-labeled anti-mouse B220 (eBioscience) and biotin-conjugated peanut agglutinin (PNA; Vector Laboratories) followed by FITC-conjugated Streptavidin (eBioscience), and visualized by microscopy as above.

**Flow cytometry.** Suspensions of peripheral blood leukocytes or splenocytes were subjected to red blood cell lysis, washed, and stained with directly conjugated fluorescent antibodies to the indicated surface markers (eBioscience). The protocol for analysis of LacZ expression was adapted from (Guo and Wu, 2008). Briefly, single cell suspensions were washed and resuspended in HBSS with 1 mM HEPES and 2% FBS, incubated for 20 min at 37°C, mixed with pre-warmed 2 mM fluorescein di-β-D-galactopyranoside (FDG, SigmaAldrich) in a hypotonic solution for 1 min, placed on ice and washed with ice-cold HBSS buffer. Endogenous β-gal activity from lysosomes was inhibited by 0.3 mM chloroquine diphosphate. Following FDG loading, cells were stained for surface markers and analyzed by flow cytometry. Samples were acquired on the LSR II (BD) or Attune NxT (ThermoFisher) flow cytometers and analyzed using FlowJo software (Tree Star).

**Autoreactive antibody clones.** MAbs derived from mice with SLE included PR1-3 (anti-DNA/histone H2a/H2b), PL2-8 (anti-DNA/histone), PL9-11 (anti-DNA)

(Losman et al., 1993; Monestier and Novick, 1996) and 3H9 (anti-DNA) (Shlomchik et al., 1987). These mAbs were kindly provided M. Shlomchik (University of Pittsburgh) and used as hybridoma supernatants for staining, except for PR1-3 which was used as a purified IgG. MAbs carrying the 9G4 idiotope derived from human SLE patients have been described (Jenks et al., 2013; Richardson et al., 2013; Tipton et al., 2015) and were used as purified IgG.

**Histopathology.** Sections of formalin-fixed kidneys (2  $\mu$ m) were stained with H&E and evaluated by a pathologist (V. D'Agati) who was blinded to sample identity. Mesangial and endocapillary proliferation, leukocyte infiltration, glomerular deposition, and apoptosis were scored separately on a scale from 0 (none) to 4 (highest) and added to yield a cumulative score. The percentage of cortical parenchyma with interstitial inflammation was also determined. Images were captured on Zeiss AxioImager upright microscope and processed by AxioVision software (Carl Zeiss).

**Molecular modeling.** ZEGA global sequence alignment of DNASE1 (PDB:2DNJ, chain a) and DNASE1L3 (Uniprot:Q13609) was performed as previously described (Abagyan and Batalov, 1997). 3D structures were visualized and analyzed with Internal Coordinate Mechanics Software (ICM-Pro Molsoft LLC, La Jolla, CA). Amino acids in the DNASE1 crystal structure 2DNJ, chain a contacting DNA were identified by selecting amino acids exhibiting any atom center within a 5 Å radius of any atom center in the DNA. Prediction of the structure of the isolated DNASE1L3 C-terminus (282-SSRAFTNSKKSIVTLRKKTKSKRS-305 ) and the C-terminus and His mutants in the context of the whole DNASE1L3 protein was performed using the Biased-Probability Monte Carlo algorithm, which was shown to be as accurate as experimental structure determination for short peptides (Abagyan and Totrov, 1994). Homology modeling of DNASE1L3 was performed as previously described (Cardozo et al., 1995).

#### **PCR primer sequences**

GFP

FW: AAGTTCATCTGCACCACCGG, RV: GCGCTCCTGGACGTAGCCTT

Human *Alu* repeats:

FW: TCACGCCTGTAATCCCAGCA, RV: AGCTGGGACTACAGGCGCCC

Mouse *B1* repeats:

FW: GGGCATGGTGGCGCACGCCT, RV: GAGACAGGGTTTCTCTGTGT

## Supplemental References

- Abagyan, R., and Totrov, M. (1994). Biased probability Monte Carlo conformational searches and electrostatic calculations for peptides and proteins. *J Mol Biol* 235, 983-1002.
- Abagyan, R.A., and Batalov, S. (1997). Do aligned sequences share the same fold? *J Mol Biol* 273, 355-368.
- Blanco, F., Kalsi, J., and Isenberg, D.A. (1991). Analysis of antibodies to RNA in patients with systemic lupus erythematosus and other autoimmune rheumatic diseases. *Clin Exp Immunol* 86, 66-70.
- Buch, T., Heppner, F.L., Tertilt, C., Heinen, T.J., Kremer, M., Wunderlich, F.T., Jung, S., and Waisman, A. (2005). A Cre-inducible diphtheria toxin receptor mediates cell lineage ablation after toxin administration. *Nature methods* 2, 419-426.
- Cardozo, T., Totrov, M., and Abagyan, R. (1995). Homology modeling by the ICM method. *Proteins* 23, 403-414.
- Caton, M.L., Smith-Raska, M.R., and Reizis, B. (2007). Notch-RBP-J signaling controls the homeostasis of CD8- dendritic cells in the spleen. *J Exp Med* 204, 1653-1664.
- Giltiay, N.V., Chappell, C.P., Sun, X., Kolhatkar, N., Teal, T.H., Wiedeman, A.E., Kim, J., Tanaka, L., Buechler, M.B., Hamerman, J.A., et al. (2013). Overexpression of TLR7 promotes cell-intrinsic expansion and autoantibody production by transitional T1 B cells. *J Exp Med* 210, 2773-2789.
- Guo, W., and Wu, H. (2008). Detection of LacZ expression by FACS-Gal analysis. *Nature Protocol Exchange*.
- Hashimoto, D., Chow, A., Greter, M., Saenger, Y., Kwan, W.H., Leboeuf, M., Ginhoux, F., Ochando, J.C., Kunisaki, Y., van Rooijen, N., et al. (2011). Pretransplant CSF-1 therapy expands recipient macrophages and ameliorates GVHD after allogeneic hematopoietic cell transplantation. *J Exp Med* 208, 1069-1082.
- Heng, T.S., and Painter, M.W. (2008). The Immunological Genome Project: networks of gene expression in immune cells. *Nat Immunol* 9, 1091-1094.
- Hochberg, M.C. (1997). Updating the American College of Rheumatology revised criteria for the classification of systemic lupus erythematosus. *Arthritis Rheum* 40, 1725.
- Jenks, S.A., Palmer, E.M., Marin, E.Y., Hartson, L., Chida, A.S., Richardson, C., and Sanz, I. (2013). 9G4+ autoantibodies are an important source of apoptotic cell reactivity associated with high levels of disease activity in systemic lupus erythematosus. *Arthritis Rheum* 65, 3165-3175.
- Losman, M.J., Fasy, T.M., Novick, K.E., and Monestier, M. (1993). Relationships among antinuclear antibodies from autoimmune MRL mice reacting with histone H2A-H2B dimers and DNA. *International immunology* 5, 513-523.
- Mabbott, N.A., Baillie, J.K., Brown, H., Freeman, T.C., and Hume, D.A. (2013). An expression atlas of human primary cells: inference of gene function from coexpression networks. *BMC Genomics* 14, 632.
- Monestier, M., and Novick, K.E. (1996). Specificities and genetic characteristics of nucleosome-reactive antibodies from autoimmune mice. *Mol Immunol* 33, 89-99.
- Ozcakar, Z.B., Foster, J., 2nd, Diaz-Horta, O., Kasapcopur, O., Fan, Y.S., Yalcinkaya, F., and Tekin, M. (2013). DNASE1L3 mutations in hypocomplementemic urticarial vasculitis syndrome. *Arthritis Rheum* 65, 2183-2189.

- Quintana, F.J., Hagedorn, P.H., Elizur, G., Merbl, Y., Domany, E., and Cohen, I.R. (2004). Functional immunomics: microarray analysis of IgG autoantibody repertoires predicts the future response of mice to induced diabetes. *Proc Natl Acad Sci U S A* 101 Suppl 2, 14615-14621.
- Richardson, C., Chida, A.S., Adlowitz, D., Silver, L., Fox, E., Jenks, S.A., Palmer, E., Wang, Y., Heimbarg-Molinaro, J., Li, Q.Z., et al. (2013). Molecular basis of 9G4 B cell autoreactivity in human systemic lupus erythematosus. *J Immunol* 191, 4926-4939.
- Sharov, A.A., Dudekula, D.B., and Ko, M.S. (2005). A web-based tool for principal component and significance analysis of microarray data. *Bioinformatics* 21, 2548-2549.
- Shlomchik, M.J., Aucoin, A.H., Pisetsky, D.S., and Weigert, M.G. (1987). Structure and function of anti-DNA autoantibodies derived from a single autoimmune mouse. *Proc Natl Acad Sci U S A* 84, 9150-9154.
- Sudo, T., Nishikawa, S., Ogawa, M., Kataoka, H., Ohno, N., Izawa, A., Hayashi, S., and Nishikawa, S. (1995). Functional hierarchy of c-kit and c-fms in intramarrow production of CFU-M. *Oncogene* 11, 2469-2476.
- Tipton, C.M., Fucile, C.F., Darce, J., Chida, A., Ichikawa, T., Gregoret, I., Schieferl, S., Hom, J., Jenks, S., Feldman, R.J., et al. (2015). Diversity, cellular origin and autoreactivity of antibody-secreting cell population expansions in acute systemic lupus erythematosus. *Nat Immunol* 16, 755-765.
- Wu, H.Y., Quintana, F.J., and Weiner, H.L. (2008). Nasal anti-CD3 antibody ameliorates lupus by inducing an IL-10-secreting CD4<sup>+</sup> CD25<sup>-</sup> LAP<sup>+</sup> regulatory T cell and is associated with down-regulation of IL-17<sup>+</sup> CD4<sup>+</sup> ICOS<sup>+</sup> CXCR5<sup>+</sup> follicular helper T cells. *J Immunol* 181, 6038-6050.
- Yogev, N., Frommer, F., Lukas, D., Kautz-Neu, K., Karam, K., Ielo, D., von Stebut, E., Probst, H.C., van den Broek, M., Riethmacher, D., et al. (2012). Dendritic cells ameliorate autoimmunity in the CNS by controlling the homeostasis of PD-1 receptor(+) regulatory T cells. *Immunity* 37, 264-275.

**Figure S1, related to Fig. 1. Characterization of *Dnase1/3*-deficient mice**

(A) Targeting strategy for the generation of *Dnase1/3*-deficient mice. Coding exons 3 and 4 of *Dnase1/3* have been replaced with a LacZ cassette in the sense orientation and the selection cassette in antisense orientation.

(B) Levels of total IgA, IgM, IgG, and IgG subclasses in WT or KO mice on indicated backgrounds at 40 weeks of age as measured by ELISA.

(C) Levels of anti-RNA IgG in the sera of WT or KO mice of indicated ages as measured by ELISA.

(D) The repertoire of autoreactive IgG in the sera of WT or KO mice as examined by antigen microarray. Sera of WT (n=3) or KO (n=5) mice on a129 background were incubated with antigen microarrays, and signals of IgG bound to individual antigens were determined. Shown are pairwise comparisons of average signals for each antigen probe at the indicated three time points; probes with >1.5-fold higher signal in WT or KO are highlighted in red or green, respectively.

(E) IgM and IgG autoreactivity of 40 weeks old WT (n=3) and *Dnase1/3* KO (n=5) mice as measured by an antigen array. Shown are heat maps of the relative IgM and IgG seroreactivity to the indicated autoantigens.

(F) Serum titers of anti-chondroitin IgG in WT or KO mice of the 129 backgrounds at the indicated time points as determined by ELISA.

Statistical significance is indicated as follows: \*,  $P \leq 0.05$ ; \*\*,  $P \leq 0.01$ ; \*\*\*,  $P \leq 0.001$ .

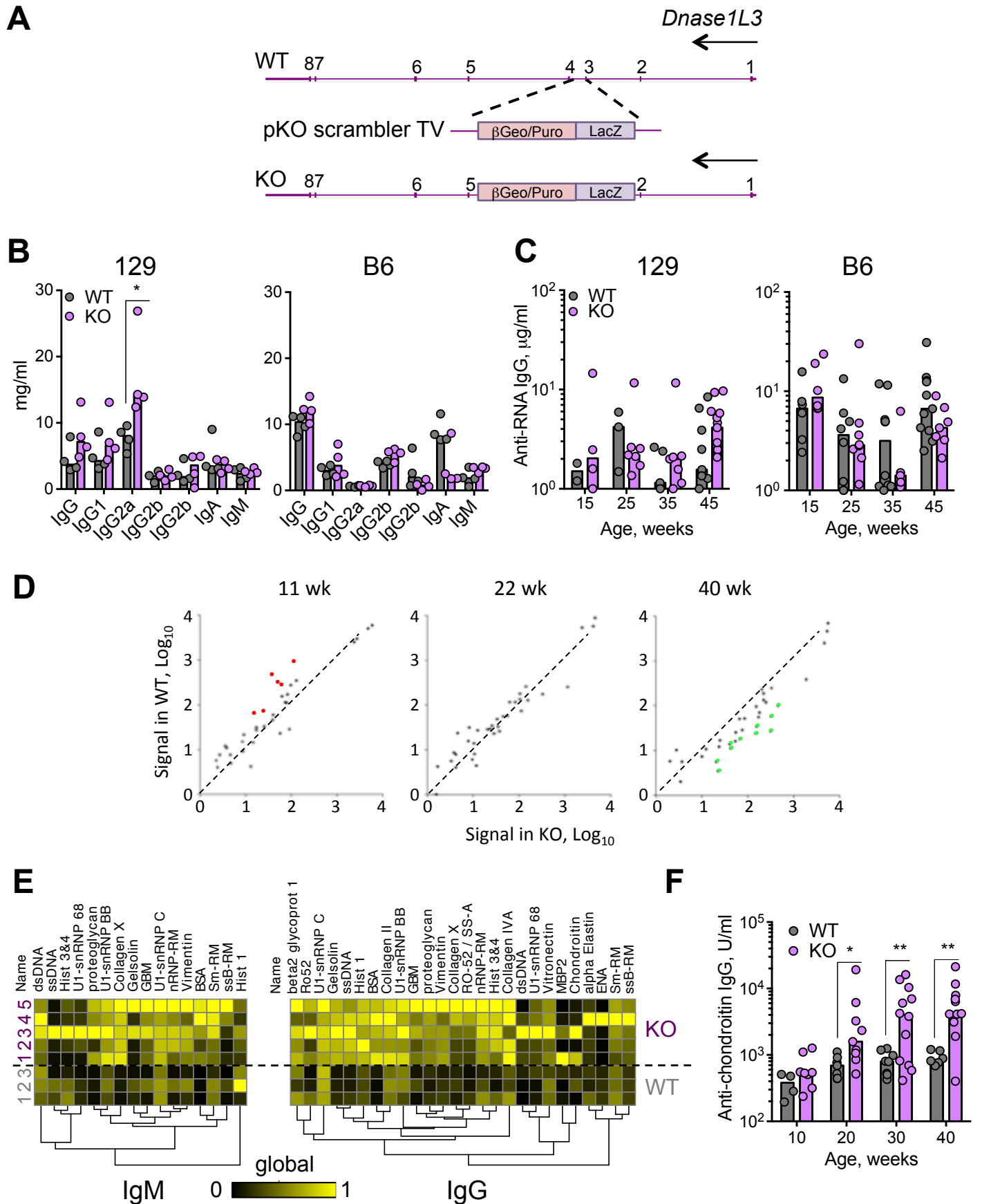


**Fig. S1**

**Figure S2, related to Fig. 2. Immune activation in *Dnase1/3*-deficient mice and its acceleration by type I IFN**

(A-C) Immune activation phenotype of control (WT) and *Dnase1/3* knockout (KO) mice. Splenic cell suspensions at indicated time points were analyzed by flow cytometry for the frequencies of (A) marginal zone B cells (MZB, B220<sup>+</sup> AA4.1<sup>-</sup> CD23<sup>-</sup> CD21<sup>+</sup>) among B cells; (B) monocytes (CD11c<sup>-</sup> Gr1<sup>-</sup> CD11b<sup>+</sup>) among live splenocytes; and (C) activated CD4 T cells (CD4<sup>+</sup> CD44<sup>+</sup> CD45RB<sup>-</sup>) among CD4<sup>+</sup> T cells. Shown are results from individual mice (circles) and the median (bar).

(D-J) The effect of adenoviral type I IFN expression on autoimmunity in *Dnase1/3* KO mice. Young 5-week-old KO or WT mice on the B6 background were injected with adenoviral vector encoding IFN- $\alpha$ 5 and analyzed at the indicated time points post-injection.

(D) The concentration of IFN $\alpha$  in the sera as measured by ELISA.

(E) The expression of IFN-inducible marker Sca-1 on B cells from peripheral blood as measured by flow cytometry.

(F) The titers of anti-dsDNA IgG as determined by ELISA.

(G) The titers of anti-RNA IgG as determined by ELISA.

(H) The frequency of monocytes (CD11c<sup>+</sup> CD11b<sup>+</sup> MHC cl II<sup>-</sup>) among peripheral blood mononuclear cells (median + range of 7 animals).

(I) The frequency of activated CD4<sup>+</sup> T cells (CD44<sup>+</sup> CD45RB<sup>-</sup>) among peripheral blood T cells (median + range of 7 animals).

(J) Kaplan-Meier survival plot (n=10/genotype). Significance was determined by a log rank test.

Statistical significance is indicated as follows: \*,  $P \leq 0.05$ ; \*\*,  $P \leq 0.01$ ; \*\*\*,  $P \leq 0.001$ .

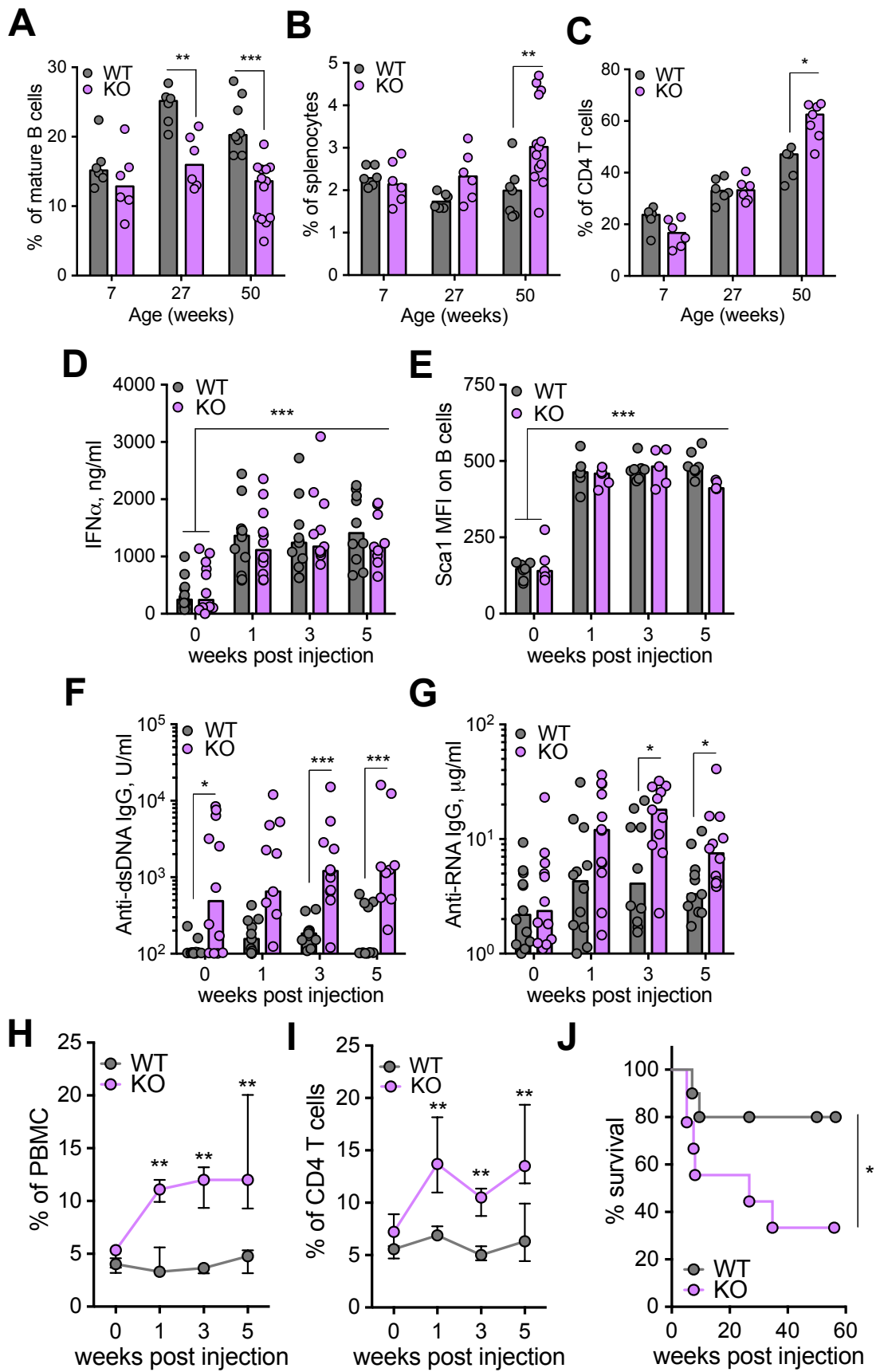


Fig. S2

**Figure S3, related to Fig. 3. Characterization of autoimmunity in bone marrow chimeras.**

(A) Quantitative analysis of Dnase1L3 activity in the mouse serum. Sera from WT, KO or heterozygous (Het) animals were tested for the ability to digest liposome-bound plasmid DNA. Shown is relative DNASE1L3 activity in individual animals (circles); bars indicate the median.

(B-D) Autoreactivity in reciprocal bone marrow (BM) chimeras. *Dnase1/3* KO animals or WT controls were lethally irradiated and reconstituted with WT or KO BM, generating two experimental (KO-to-WT and WT-to-KO) and two control (KO-to-KO and WT-to-WT) types of chimeras.

(B) Serum DNASE1L3 activity in the four chimera types at the indicated time points after reconstitution (mean  $\pm$  SD of 6 to 8 animals per group).

(C) Anti-dsDNA IgG antibody-secreting cells (ASC) in the spleens of BM chimeras as determined by ELISPOT at 55 weeks post-reconstitution (ASC per  $10^6$  splenocytes).

(D) ANA in the sera of BM chimeras 55 weeks post-reconstitution.

(E-F) Autoreactivity in BM chimeras with a complete hematopoietic reconstitution. WT mice were lethally irradiated and reconstituted with WT or KO BM. The KO-to-WT chimeras showed nearly complete donor reconstitution, loss of serum DNASE1L3, anti-dsDNA IgG and ANA (Fig. 3F-H). The chimeras were analyzed 55 week post-reconstitution.

(E) IgG deposition in the kidneys. Shown are kidney sections stained by immunofluorescence for IgG and DNA (representative of 5 animals per group), and the percentage of kidney glomeruli with IgG deposits (out of 40 glomeruli per kidney of individual mice).

(F) Kidney pathology in chimeric mice. Shown are kidney sections stained with H&E (scale bars, 50  $\mu$ m) with a representative glomerulus in the inset (representative of 6 animals per group). Also shown is the histopathological score of glomerulonephritis, including the percentage of kidney cortex affected by inflammation and the median cumulative score of glomerulonephritis.

Statistical significance is indicated as follows: \*,  $P \leq 0.05$ ; \*\*,  $P \leq 0.01$ ; \*\*\*,  $P \leq 0.001$ .

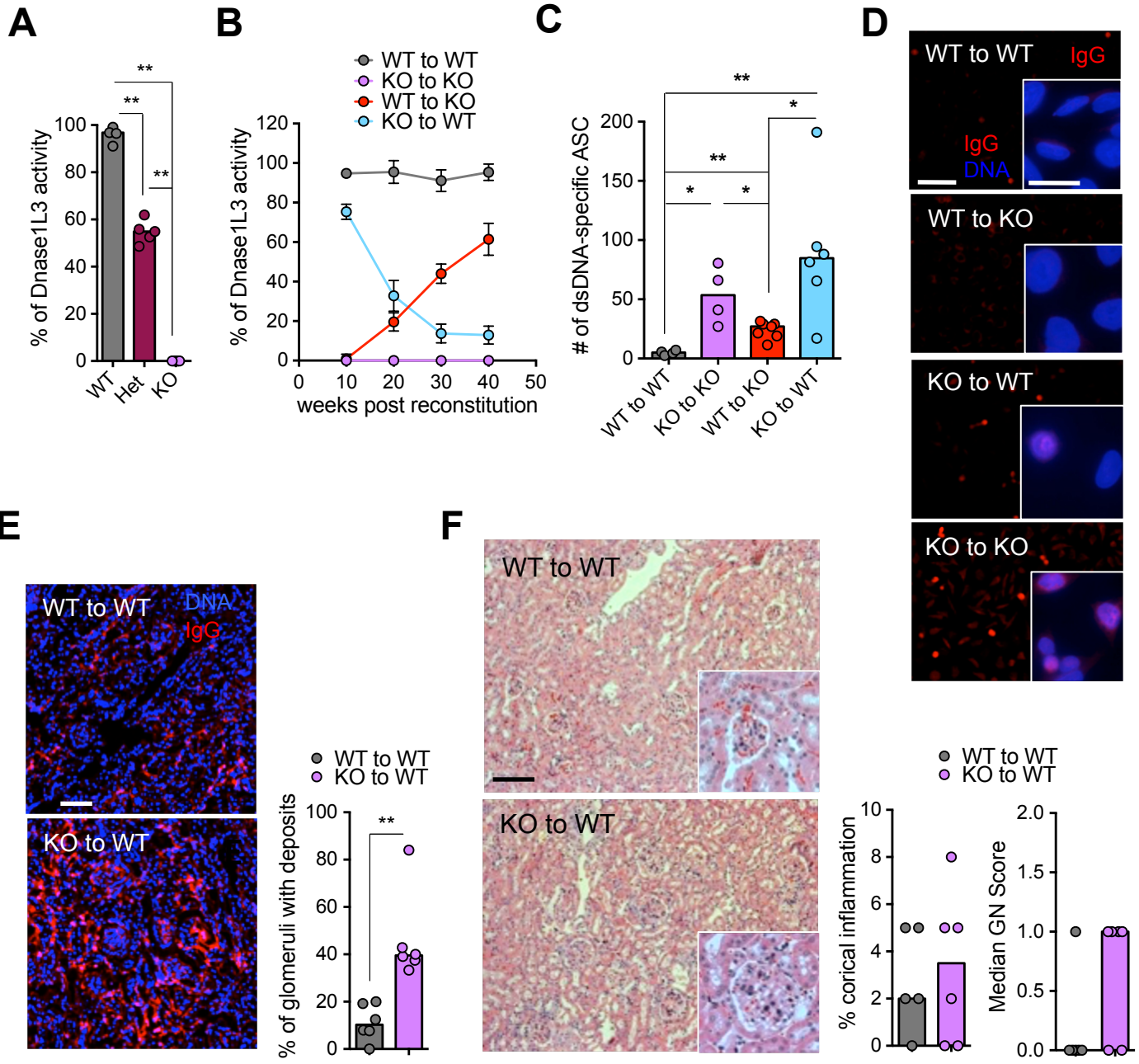


**Fig. S3**

**Figure S4, related to Fig. 4. The expression of *Dnase1/3* in murine and human tissues.**

(A) The expression of *DNASE1L3* in human tissues and cell types. Shown is the expression profile of *DNASE1L3* (probe 205554\_s\_at) in the Primary Cell Atlas microarray expression database (Mabbott et al., 2013) as visualized by the BioGPS browser (biogps.org), with the relevant cell types indicated.

(B) The expression of *Dnase1/3* in murine immune cell types. Shown is the expression profile of *Dnase1/3* in the Immgen microarray expression database (Heng and Painter, 2008) of key populations (top) and monocytes/macrophages (bottom), with the relevant cell types indicated.

(C) The expression of *Dnase1L3* in murine splenic immune cells as determined by qRT-PCR. Shown are relative expression levels in the indicated sorted cell populations normalized to *Actb* (mean  $\pm$  SD or triplicate PCR reactions). Representative of 5 experiments.

(D) Depletion efficiency of splenic macrophages and conventional dendritic cells (cDCs) 2 and 7 days post injection with clodronate liposomes or control PBS liposomes. Shown are representative profiles of pre-gated splenic B220<sup>-</sup> Ly6G<sup>-</sup> cells with the fraction of F4/80<sup>+</sup> CD11b<sup>low</sup> macrophages and CD11c<sup>+</sup> MHC cl. II<sup>+</sup> cDCs indicated (representative of 4-6 animals per group).

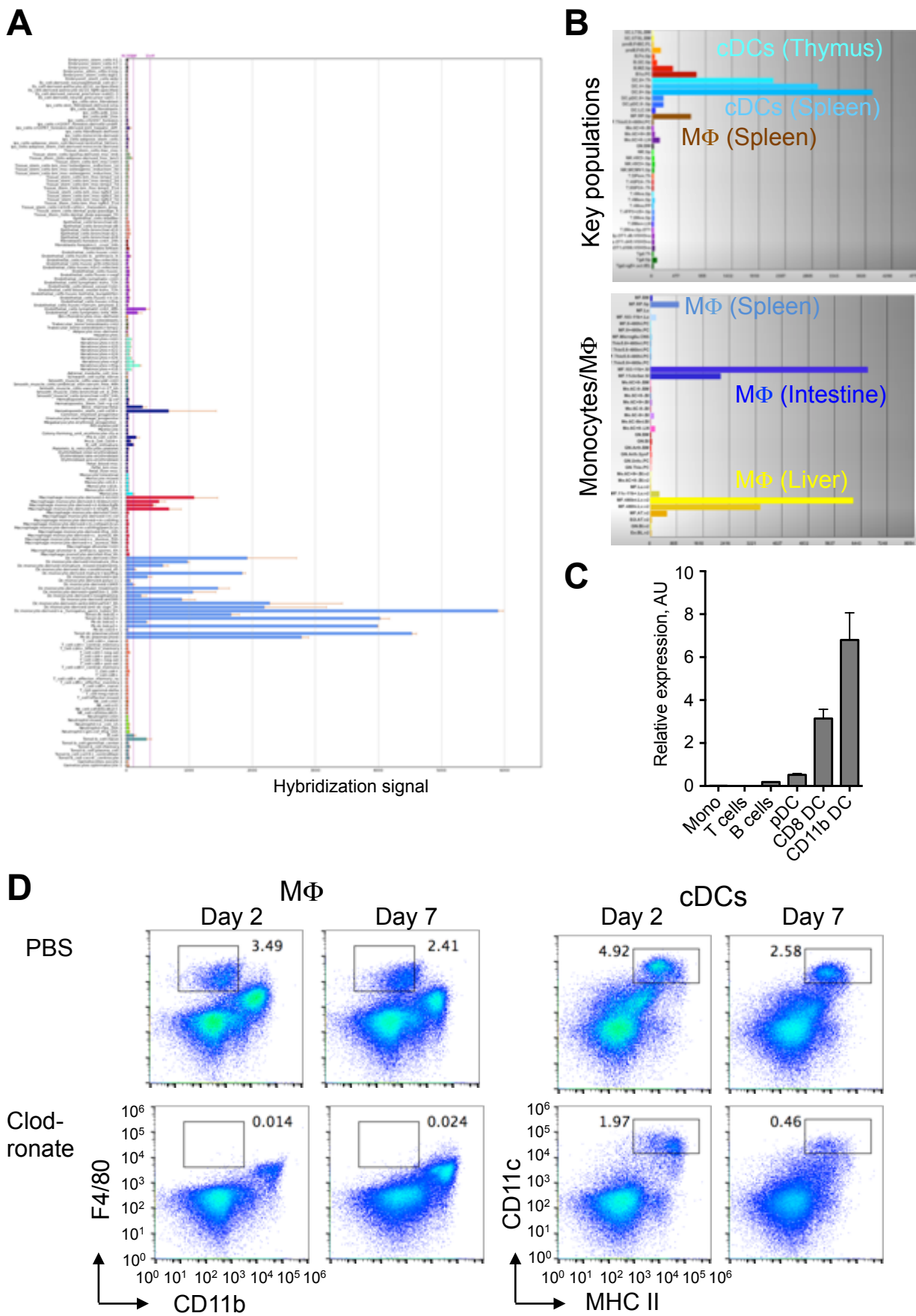


Fig. S4

**Figure S5, related to Fig. 5. Comparative structural analysis of DNASE1L3 and its mutants.**

(A) Global sequence alignment of bovine DNASE1 (PDB:2DNJ.a, top) and human DNASE1L3 (Uniprot:Q13609). Red boxes represent amino acids of DNASE1 that contact DNA and orange lines represent selected residues contacting DNA.

(B) 3D structure of the complex of DNASE1 with DNA. Selected DNA contacting residues are colored orange.

(C) *ab initio* structure prediction of the C-terminus of DNASE1L3 (a.a. 282-305). Shown is the 3D structure of the lowest energy conformation and the energy spectrum of the folding simulation. Note a ~5 energy unit (~kcal) gap between the lowest energy conformation and the first non-helical conformation, indicating a highly rigid helical structure.

(D) Homology model of DNASE1L3 based on PDB:2DNJ, with *ab initio* structure prediction of the C-terminus in situ in the whole protein. Note that the rigid  $\alpha$ -helical conformation preferred by the isolated C-terminus (Panel C) is unperturbed in the context of the whole protein.

(E) Homology model of DNASE1L3 mutants with a hexahistidine tag at the C-terminus (His-CT) or between the DNase domain and the C-terminus (His-preCT). Note that the  $\alpha$ -helical conformation of the C-terminal peptide appears unperturbed by His tags, but its C-terminus is blocked in the His-CT mutant, and its packing against the DNase domain is altered in the His-preCT mutant.

(F) Time-dependent digestion of nucleosomal DNA by sera from *Dnase1/3*-deficient animals. Purified HeLa polynucleosomes were incubated with sera from control (WT) or *Dnase1/3* KO animals, and the amount of remaining DNA was measured by qPCR. Shown is the % input DNA at the indicated time points (representative of 3 experiments).

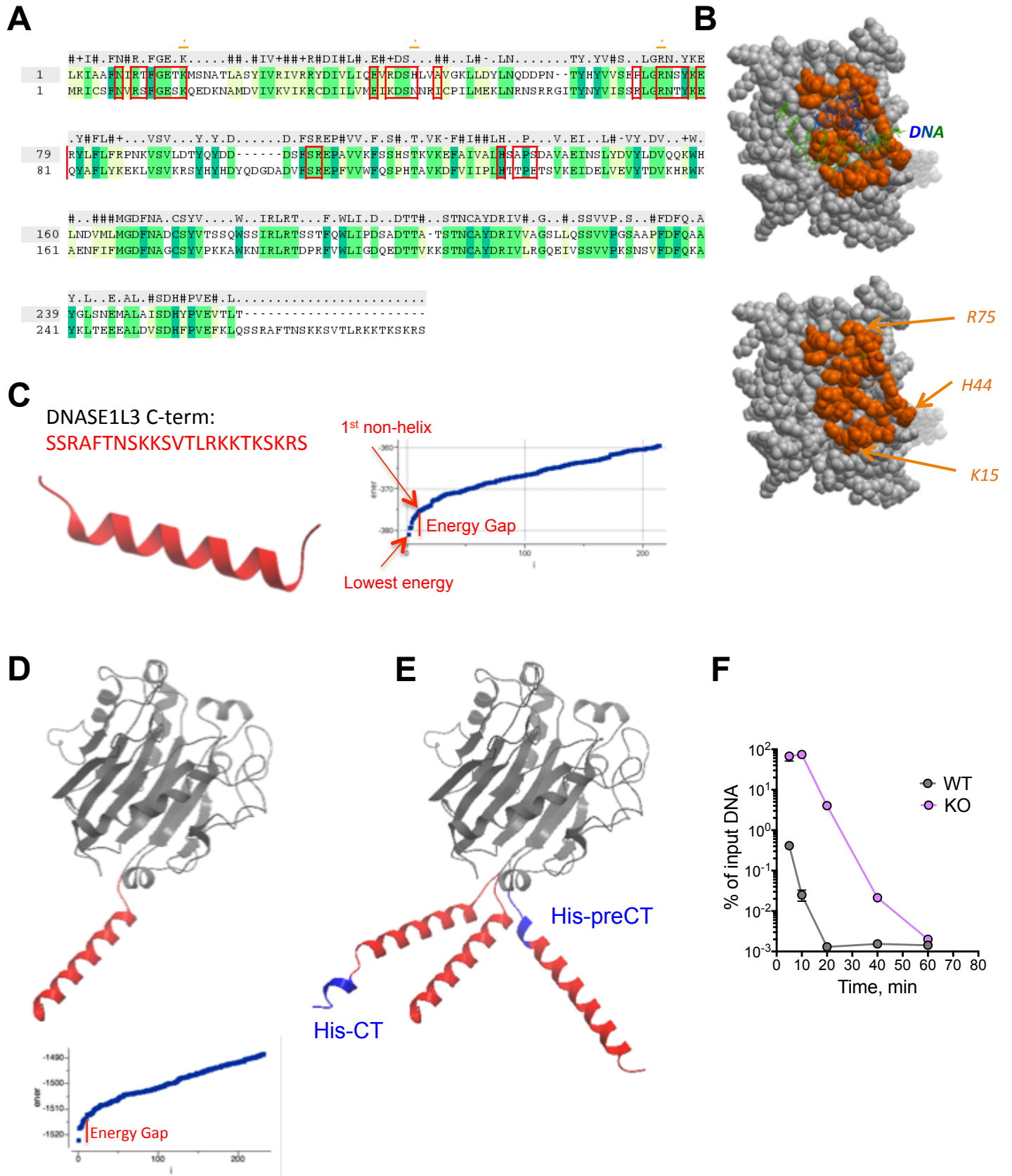


Fig. S5

**Figure S6, related to Fig. 6. Characterization of murine and human microparticles**

(A) Persistence of DNA in apoptotic cell microparticles *in vivo*. Wild-type (WT) or *Dnase1/3* knockout (KO) mice were injected i.v. with Jurkat cell microparticles (MP) and sacrificed 3, 24 or 48 hr later. The concentration of human genomic DNA in the indicated tissues was determined 3, 24 or 48 hr later and expressed as amounts of DNA in input MP per volume of serum or of tissue lysate. Shown are results from individual mice (circles) and the median (bar).

(B) The phenotype of endogenous circulating microparticles in the mouse. Mouse MP from plasma were enriched by differential centrifugation and stained for platelet and red blood cell markers (CD41 and Ter119, respectively) in the same channel. MP were defined as FSC<sup>lo</sup> SSC<sup>lo</sup> CD41<sup>-</sup> Ter119<sup>-</sup>. Shown is a representative staining of mouse plasma MP for apoptotic cell marker Annexin V and endothelial marker CD31.

(C) The number of circulating MP in the plasma of WT and KO animals as determined by flow cytometry.

(D) The phenotype of endogenous circulating microparticles in the human. Human MP from plasma were enriched by differential centrifugation and stained for platelet and red blood cell markers (CD42b and CD235a, respectively). MP were defined as FSC<sup>lo</sup> SSC<sup>lo</sup> CD42b<sup>-</sup> CD235a<sup>-</sup>. Shown are representative stainings of human plasma MP for Annexin V versus endothelial marker CD31, leukocyte marker CD45 or granulocyte marker CD66b.

(E) The partition of genomic DNA between the microparticle fraction and the soluble fraction of human plasma. The amount of genomic DNA was measured by qPCR in unfractionated human plasma, the microparticle-containing fraction obtained by centrifugation, or in the remaining soluble fraction. Shown are DNA amounts per  $\mu\text{l}$  of the original unfractionated plasma volume in samples from individual SLE patients (n=8) or healthy controls (n=2).

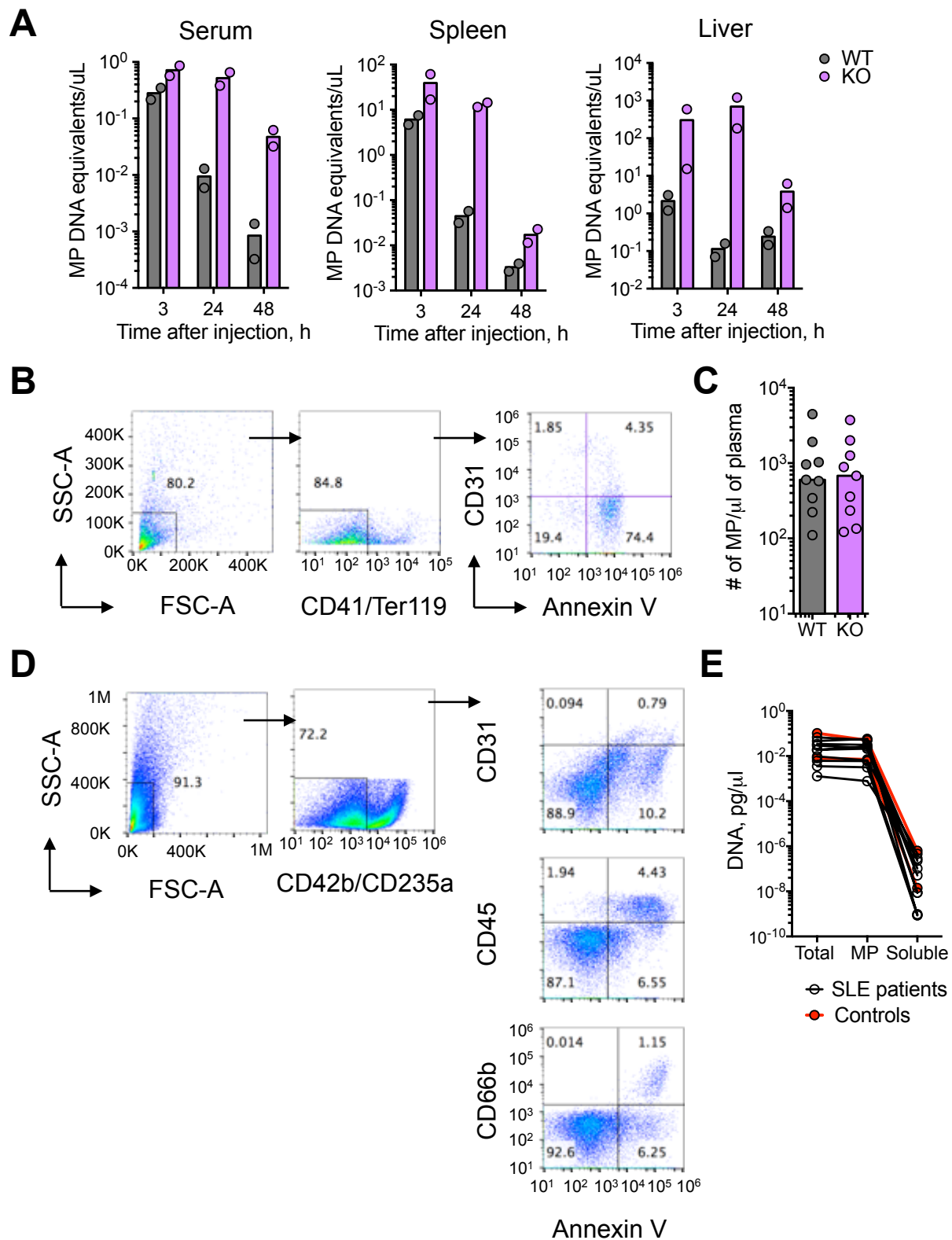


Fig. S6

**Figure S7, related to Fig. 7. DNASE1L3-sensitive binding of anti-DNA antibodies to microparticles**

(A) Binding of murine anti-DNA mAbs to the surface of microparticles. Microparticles (MP) from apoptotic human Jurkat cells were incubated with supernatants containing human DNASE1 or DNASE1L3 or an empty control and stained with murine anti-DNA mAbs followed by secondary anti-mouse IgG fluorescent antibody. Shown are fluorescence signals of the indicated mAbs and the % of positive MP; representative of 3 experiments.

(B) Binding of human 9G4<sup>+</sup> mAbs to the surface of microparticles. MP from apoptotic human Jurkat cells were incubated with supernatants containing human DNASE1L3 or an empty control and stained with human 9G4<sup>+</sup> mAbs followed by secondary anti-human IgG fluorescent antibody. Shown are fluorescence signals of the indicated mAbs and the % of positive MP; representative of 2 experiments.

(C-D) The binding of serum IgG from patients with sporadic SLE to microparticles. Microparticles (MP) from apoptotic human Jurkat cells were incubated with supernatants containing DNASE1L3 or an empty control (untreated) and stained with sera or plasma from SLE patients followed by secondary anti-human IgG fluorescent antibody.

(D) The definition of positive binding to native MP. Shown is the total mean fluorescent intensity (MFI) of IgG fluorescence versus the % of positively stained MP for each sample. Positive binding was defined as >5% IgG<sup>+</sup> MP (green circles).

(D) DNASE1L3 sensitivity of serum IgG binding to microparticles. For samples showing positive binding as defined in panel D, shown is the % of positively stained untreated MP vs the relative of change in the binding to DNASE1L3-treated MP. Samples above the trend line were defined as showing DNASE1L3-sensitive binding (red circles). Similar results were obtained using chi-square or Kolmogorov-Smirnov statistics to estimate differences between empty and DNASE1L3-treated MP staining (data not shown).

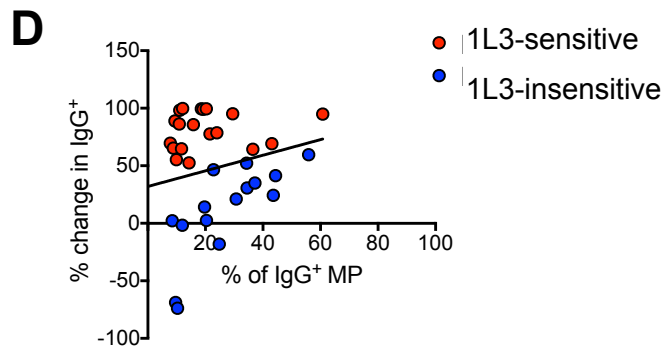
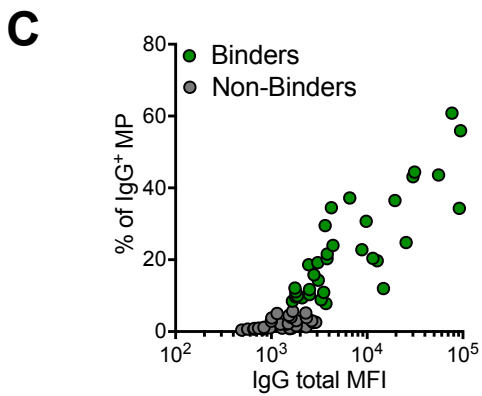
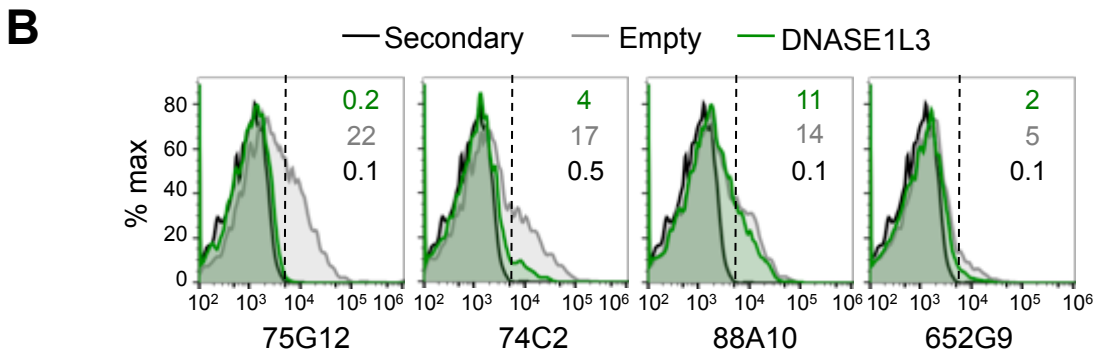
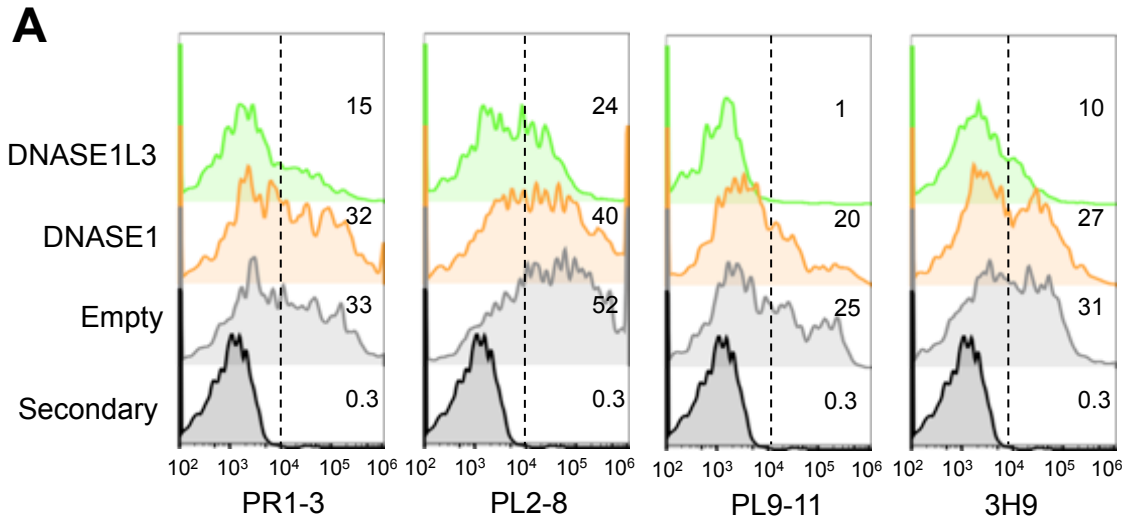


Fig. S7